



# Aeolian–lacustrine margins: implications for carbon capture and storage within the Rotliegend Group, Southern North Sea

Charlotte L. Priddy<sup>1\*</sup>, Ross P. Pettigrew<sup>2</sup>, Douglas Watson<sup>1</sup>, Amy V. Regis<sup>2</sup> and Stuart M. Clarke<sup>2</sup>

<sup>1</sup> Department of Geology & Geophysics, School of Geosciences, University of Aberdeen, Aberdeen AB24 3UE, Scotland, UK

<sup>2</sup> Basin Dynamics Research Group, School of Geography, Geology and the Environment, Keele University, Keele ST5 5BG, UK

CLP, 0000-0002-3007-1374; RPP, 0000-0001-5664-6765; DW, 0000-0001-9575-3141

\* Correspondence: [charlotte.priddy@abdn.ac.uk](mailto:charlotte.priddy@abdn.ac.uk)

**Abstract:** The Southern North Sea Basins of the United Kingdom were renowned for their hydrocarbon resources and exploited extensively from the 1960s to the 1990s. The Permian Leman Sandstone in particular formed an excellent reservoir due to its extensive clean aeolian sediments and was subsequently explored for decades, resulting in a wealth of subsurface data that are now widely accessible. The strata of the Leman Sandstone comprises mixed continental deposits from aeolian, fluvial and lacustrine environments which interfinger with the saline lake deposits of the Silverpit Formation. With the potential reassessment of depleted gas reservoirs in the North Sea for use as sequestration targets for captured carbon dioxide, there is significant renewed interest in the reservoir geology of the Leman Sandstone. A regional study of the sedimentology and petrophysical properties of the Leman Sandstone and Silverpit formations within quadrants 43, 44, 48 and 49 of the Southern North Sea has been conducted. Multiple interactions between the depositional environments are observed, resulting in a complex interplay between aeolian and lacustrine transgressive/regressive events, and migration and expansion/contraction of the fluvial system. In wireline petrophysical data, each depositional environment, along with their transitional environments, form relatively distinct clusters that can be used as a predictive tool for reservoir interpretation in the absence of core, despite extensive sediment recycling between environments.

**Received** 31 August 2023; **revised** 9 November 2023; **accepted** 9 November 2023

Carbon capture and storage (CCS) is one of the many low carbon initiatives used to help reduce carbon emissions, in the aim to tackle global warming. With increasing interest in CCS to help meet ‘net-zero’ targets, the North Sea Transition Authority (NSTA) launched a carbon storage licensing round within the North Sea in June 2022, with 21 licences being awarded in September 2023 (NSTA 2022, 2023).

Once prime targets for hydrocarbon exploration, the arid continental strata of the Southern North Sea now present new opportunities for a low carbon future. Exploration for gas within the Triassic, Permian, and Carboniferous continental strata began in the 1960s in the Southern North Sea (SNS), with particular focus on the strata of the Permian Rotliegend Group that comprise sediments deposited within arid continental fluvial, aeolian and lacustrine environments. Since then, new hydrocarbon production ventures have decreased, with several early fields being abandoned and decommissioned. However, there is presently renewed interest in these strata for their potential to store CO<sub>2</sub> within the reservoirs of depleted hydrocarbon fields and saline aquifers (Hollingsworth *et al.* 2022). Moreover, the wealth of data available from previous oil and gas exploration, the existing infrastructure, and the proximity to emitters onshore, particularly within the Southern North Sea, creates ample opportunity to study this area for CCS potential.

Particular focus has been paid to the Triassic Bunter Formation of the Silverpit Basin for carbon capture and storage (Gluyas and Bagudu 2020; Hollingsworth *et al.* 2022), specifically the Endurance project situated in blocks 42/25 and 43/21 (Bentham *et al.* 2017; Metcalfe *et al.* 2017; Gluyas and Bagudu 2020; Sutherland *et al.* 2022). However, licences have also been awarded for appraisal of CO<sub>2</sub> storage in the depleted Rotliegend gas fields of Viking and Victor, as part of the V Net Zero project (now renamed Viking

CCS), which has the potential to store over 300 Mt of CO<sub>2</sub> over the project’s lifetime (OGA 2021).

The extensive aeolian deposits of the Rotliegend Leman Sandstone have long been prime targets for hydrocarbon exploration due to their quartz-rich, well sorted, well-rounded sandstone composition. The interaction with fluvial and lacustrine deposits often complicate hydrocarbon recovery, with many of the more mud-rich elements acting as baffles and barriers to flow, resulting in compartmentalization and slower production rates (Eaton 2006; Jolley *et al.* 2010; Mullins *et al.* 2022). However, these issues that once complicated hydrocarbon production, can be beneficial for CCS due to increased trapping mechanisms and surface area of the CO<sub>2</sub> plumes (Sundal *et al.* 2013). Therefore, understanding the interaction between these depositional elements and the lateral and vertical extents of the baffles and barriers to flow, is critical when characterizing a reservoir for CO<sub>2</sub> storage.

This work critically evaluates the prospectivity of the Permian Leman Sandstone Formation as a potential target for carbon capture and storage, utilizing a high resolution, 3D dataset of well logs and core. In so doing, this work documents the evolution of a mixed fluvial–aeolian–lacustrine margin depositional setting, along with analysing the complex sedimentology and interactions of the deposits. Consequently, the objectives of this study are: (i) to describe the key facies associations of the preserved sediments of the aeolian, fluvial and lacustrine environments; (ii) to correlate and document the regional extents of those depositional environments; (iii) to define the key petrophysical properties of the sediments of the depositional environments; and (iv) to reconstruct refined palaeogeographical maps and depositional models of the Rotliegend Group from these analyses.

## Geological setting

During the late stages of the Variscan Orogeny, the east–west-trending, low-lying, land-locked desert basin, known as the Southern Permian Basin, developed (Glennie 1998; Underhill 2003). Through the Permian Period, the Southern Permian Basin underwent tectonic subsidence followed by prolonged thermal subsidence and NW–SE transtensional tectonics, resulting in the formation of several sub-basins (Sole Pit, Silverpit and Broad Fourteens), separated by the Cleaver Bank and Sole Pit highs (Fig. 1) (Van Hoon 1987; Underhill 2003; Gast *et al.* 2010; Hollinsworth *et al.* 2022).

The early Permian Rotliegend Group was deposited in the Southern Permian Basin unconformably overlying the Carboniferous Coal Measures (Howell and Mountney 1997). The deposits of the Group range from mixed evaporitic and clastic sediments deposited in sabkha and playa lake environments of the Silverpit Formation to coeval fluvial and aeolian sediments of the Leman Sandstone Formation (Fig. 1) (Prosser 1988). The Silverpit Formation was deposited in an extensive and intermittently expanding playa lake system with associated marginal sabkhas, fringed on its southerly and southwesterly margins by the predominantly aeolian dune fields of the Leman Sandstone (Bailey and Lloyd 2001), resulting in extensive first-order bounding surfaces produced by lacustrine transgression and regression of the Silverpit Lake towards the southerly aeolian dune fields (Howell and Mountney 1997). The aeolian dune field is periodically punctuated by fluvial corridors with ephemeral rivers flowing northwards from the Variscan highland towards the Silverpit Lake (Marie 1975). The Rotliegend Group is then overlain by the cyclical carbonate-evaporite deposits of the Upper Permian Zechstein Supergroup formed during a rapid marine transgressive event (Fig. 1) (Howell and Mountney 1997; Grant *et al.* 2019; Fyfe and Underhill 2023a, b).

### Silverpit Formation

The Silverpit Formation was deposited within a desert lake which extended east – west for 1000–1200 km from the North Sea to present-day Poland, and north – south for 200 km (Glennie 1983; Cameron *et al.* 1992). Lake-centre facies are characterized by monotonous successions of red-brown, anhydritic mudstones and grey siltstones (Cameron *et al.* 1992), while lake-margin facies comprise a complex interfingering of lacustrine, sabkha, aeolian and fluvial sediments. Lake-margin facies are up to 50 m thick, consisting of interbedded claystones, siltstones and sandstones, often in upwards fining cycles (Butler 1975). Sandstones are interpreted to have been deposited by distal sheetflood deposits entering the desert lake, with shoreline sabkha facies represented by adhesion-rippled sandstones and nodular anhydrite within claystones and siltstones (Glennie 1972). Rare interbedded aeolian and fluvial deposits indicate periods of lake retreat, however the sabkha and lacustrine deposits are gradational so the lateral limits of the sabkha facies are not easily determined (Cameron *et al.* 1992). Long-term expansion of the lake is seen within the south of the basin, as the lacustrine facies prograde over the lake margin aeolian/fluvial deposits of the Leman Sandstone Formation (Butler 1975). Short-term fluctuations are also seen within the lake-margin facies, with complex interbedding of lacustrine, sabkha, aeolian and fluvial deposits (Cameron *et al.* 1992).

### Leman Sandstone

The Leman Sandstone is composed almost entirely of aeolian and fluvial strata, which form relatively distinct packages in core and wireline logs (Glennie 1972; Cameron *et al.* 1992; Sweet 1999).

The fluvial sediments were deposited in alluvial plains and floodplains by ephemeral rivers flowing northwards from the Variscan highland towards the Silverpit desert palaeolake in the centre of the North Sea basin (Marie 1975; George and Berry 1993). Fluvial deposits comprise conglomeratic units which interfinger with red-brown sandstones and dark-red mudstones and claystones. Distinct deposits of fluvial strata are 100 m at their thickest, and intercalated with aeolian sandstones, elsewhere fluvial deposits average ~50 m in thickness (Glennie 1986). Rainfall was most likely seasonal, occurring in violent storms with floodwaters following interdune corridors between sand dunes, eroding and reworking aeolian and previously deposited fluvial sands. During dry periods aeolian sediment encroached over these wadis but did not become well-established (Marie 1975).

Aeolian sandstones dominate over the fluvial facies towards the top of the Leman Sandstone Formation, indicating a progressively drier environment through time (Cameron *et al.* 1992). Aeolian facies comprise dune sets and cosets organized into sequences up to 200 m thick. The dune sediments form the majority of the Leman Sandstone Formation strata in the east and SE area of the basin (Marie 1975; Van Veen 1975) and are interpreted to represent both transverse and seif dunes (Glennie 1972). Whereas towards the west of the basin these aeolian deposits interfinger with fluvial deposits (Glennie 1972).

## Methods

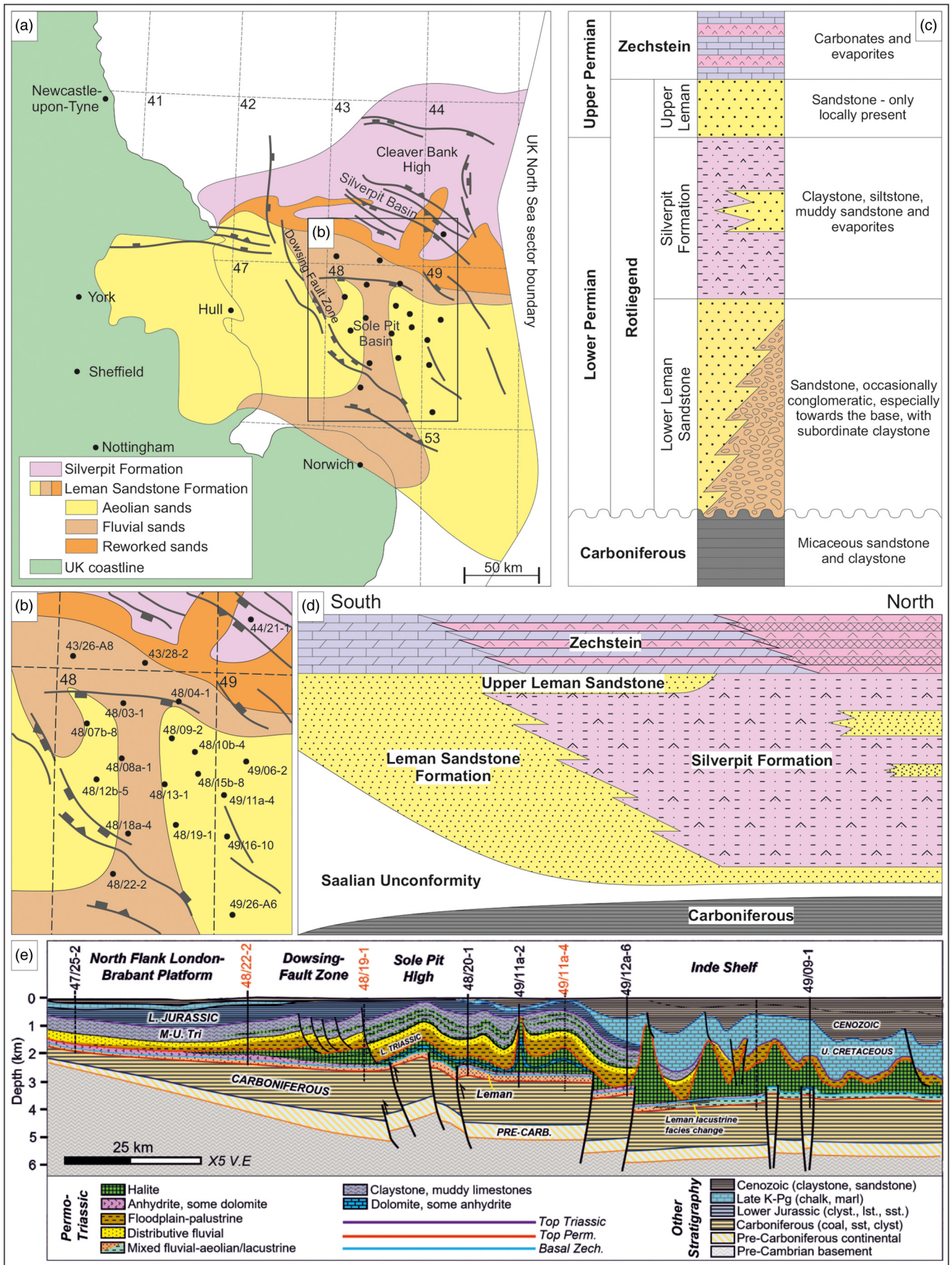
Nineteen detailed vertical sections were logged from carefully selected cored wells within quadrants 43, 44, 48 and 49 of the Southern North Sea, with a cumulative length of over 2000 m. Each well was spaced laterally by approximately 20 km over an area of roughly 50 km<sup>2</sup> and constrained to an approximate grid pattern allowing for both strike and dip cross sections through the strata (Figs 1, 2). Where possible, the core logs record full successions of the Leman Sandstone, from the unconformity with the underlying Carboniferous Coal Measures, through the Lower Leman, Silverpit Formation and Upper Leman intervals, to the overlying claystone of the Kupferschiefer.

Legacy wireline data were obtained from the UK National Data Repository (NDR), part of the North Sea Transition Authority's (NTSA) wider digital energy platform. Gamma ray, sonic, bulk density and neutron porosity data, where available, have been analysed and processed using Petrel 2020 (Schlumberger). Scrutiny of caliper measurements was conducted to ensure no significant wash out or borehole collapse was present in the sections studied for petrophysical analysis. The borehole diameters were predominantly 8½ inches but ranged from 6 inches to 12¼ inches (wells 43/26a-8 and 48/10b-4, respectively). These legacy petrophysical data have been used in combination with the sedimentary logs of the cored sections (Figs 3, 4) to identify representative wireline signatures for each facies association that characterizes each depositional environment.

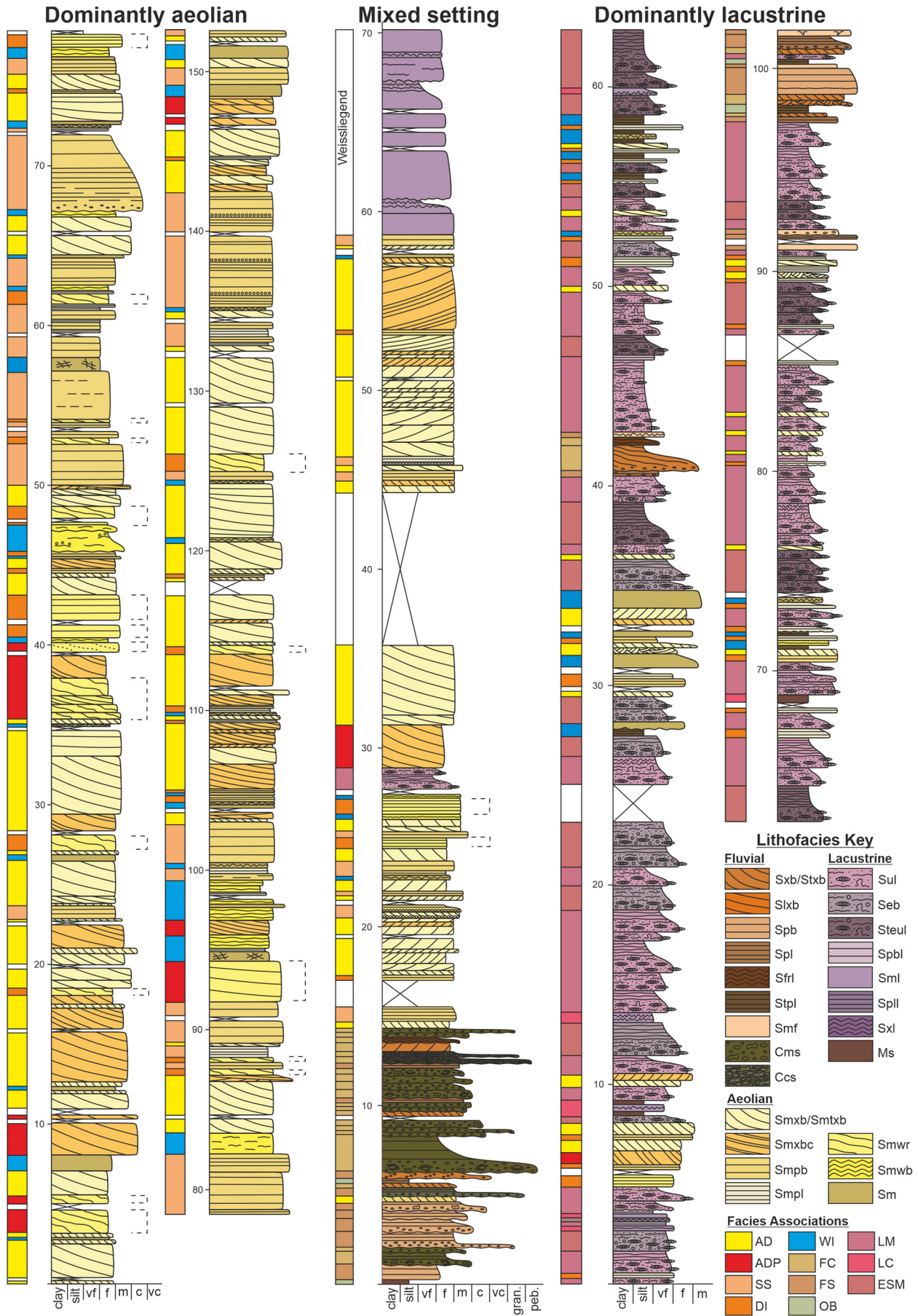
## Results

### Sedimentology

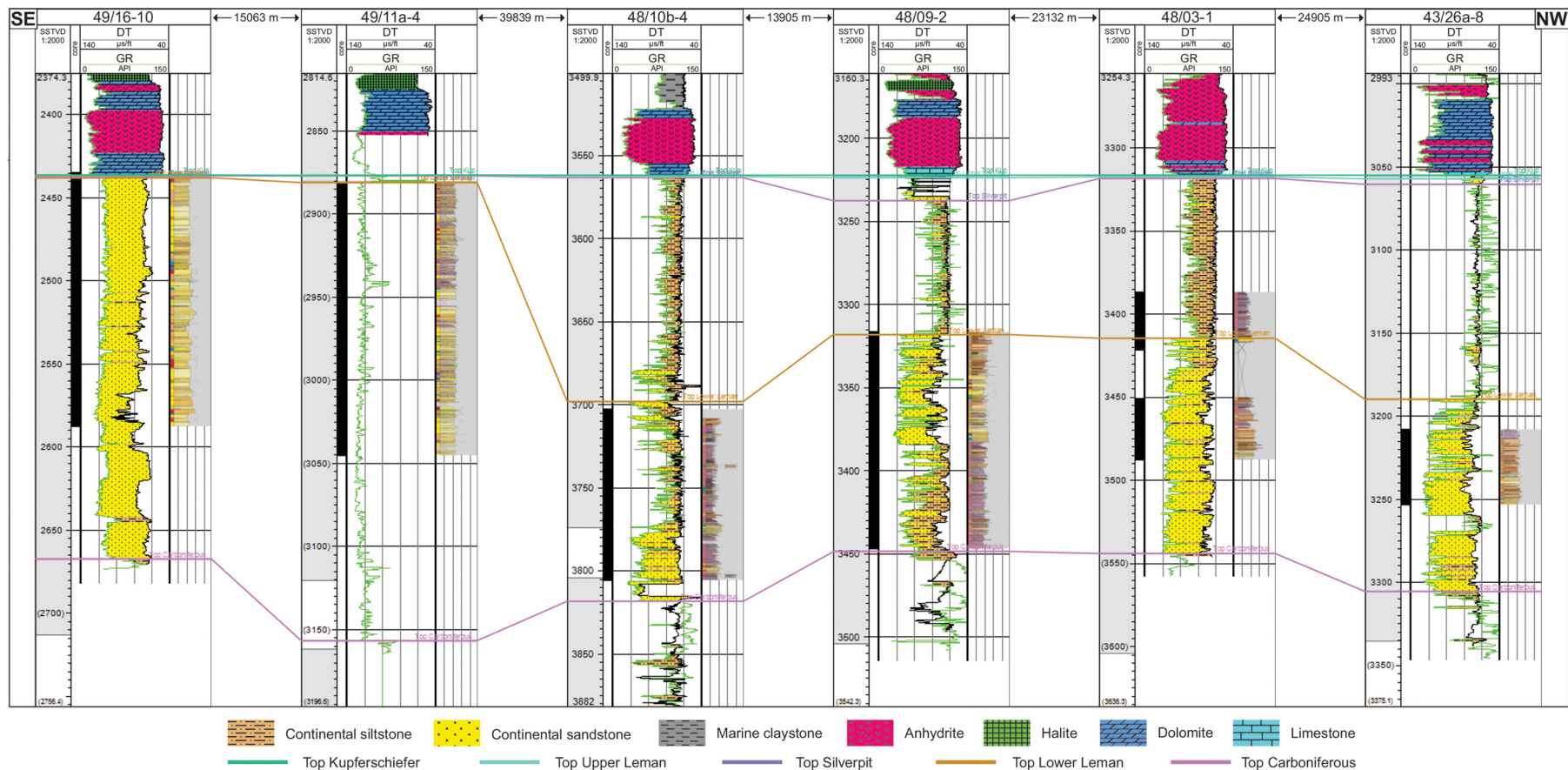
The descriptions and interpretations presented in this section are all based upon primary core observations within this study. From the 19 sedimentary logs, 26 facies are identified within the strata of the Leman Sandstone and Silverpit formations based principally upon the lithology, sedimentary textures and structures present, and they are summarized in Table 1. Eighteen facies relate to sub-aqueous processes and the remainder relate to wind-blown processes. The facies are grouped based upon depositional processes to form 11 facies associations (Table 2; Fig. 5): aeolian dune, aeolian dune



**Fig. 1.** (a) Geographical map of the east coast of the United Kingdom and Southern North Sea Basin, highlighting the extent of Lemman Sandstone and Silverpit Formation deposition, along with the location of intrabasins, highs and faults (modified after Cameron *et al.* 1992). (b) Insert map from (a) with the locations of wells studied. (c) Stratigraphic column of the Rotliegend Group (modified after Howell and Mountney 1997). (d) Regional cross-section of the Upper Rotliegend Group highlighting the relationships between the diachronous Lemman and Silverpit formations (modified after Howell and Mountney 1997). (e) Depth cross-section from seismic line, wells in red are analysed within this study.



**Fig. 2.** Selected logged section depicting the varied sedimentology of the Leman/Silverpit transition. See Tables 1 and 2 for detailed explanation of the facies and facies association codes.





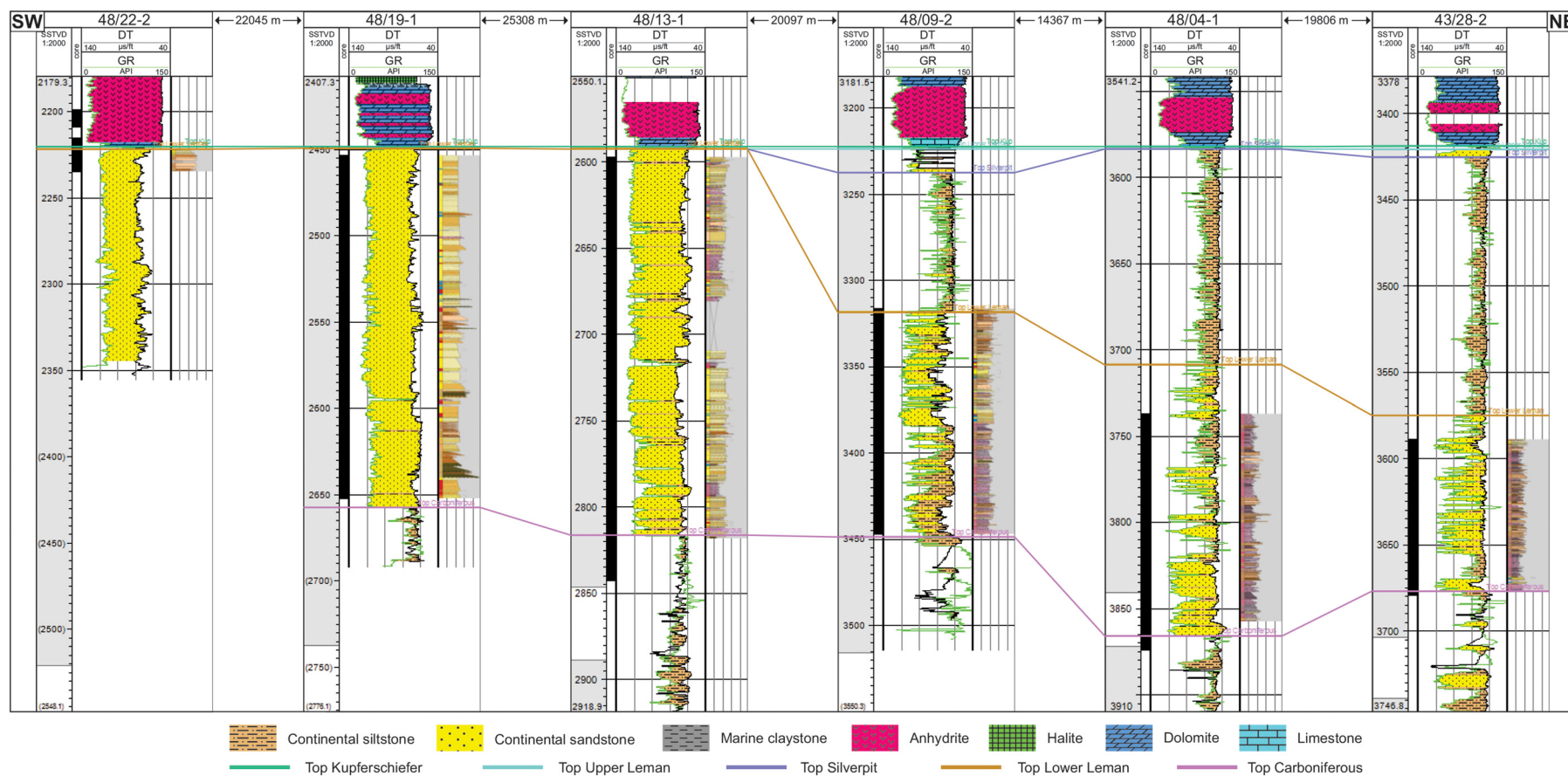





**Fig. 3.** SE to NW orientated well panel highlighting the transition of depositional environments along strike. Gamma ray signals are infilled by broad lithology and an inset image of the core logged sections for each well is included (see Fig. 2 for detailed key).



**Fig. 4.** SW to NE orientated well panel highlighting the transition of depositional environments along dip. Gamma ray signals are infilled by broad lithology and an inset image of the core logged sections for each well is included (see Fig. 2 for detailed key).

**Table 1.** Summary of lithofacies observed in the Leman and Silverpit Formations

Code	Name	Lithology & texture	Sedimentary structures	Interpretation	
<b>Smxb</b>	Planar cross-bedded sandstone		Purple-yellow-grey, medium to coarse-grained sandstone, well sorted, well-rounded	Planar cross-bedding with mm/cm scale alternations in grainsize and reverse grading	Migration of wind-blown straight-crested dune-scale bedforms formed by the avalanche of sediment down the lee slope of the dune
<b>Smxbc</b>	Planar cross-bedded sandstone couplets		Purple-yellow-grey, fine to coarse-grained sandstone, well sorted, well-rounded	Couplets of fine-grained structureless sandstone and coarser grained, reverse graded sandstone	Migration of wind-blown straight-crested dune-scale bedforms formed by the avalanche and settlement of sediment down the lee slope of the dune
<b>Smtxb</b>	Trough cross-bedded sandstone		Brown-grey, fine to medium-grained sandstone, well sorted, well-rounded	Trough cross-bedding with mm/cm scale alternations in grainsize	Migration of wind-blown sinuous-crested dune-scale bedforms
<b>Smpb</b>	Planar-bedded sandstone		Purple-grey, fine to medium-grained sandstone, well sorted, well-rounded	Planar-bedding with millimetre scale alternations in grainsize and sporadic granule-rich surfaces	Wind-blown deposits formed by the deflation of dune-scale bedforms, with evidence of deflation lags
<b>Smpl</b>	Planar laminated sandstone		Purple-grey, very-fine to medium-grained sandstone, well sorted, well-rounded	Planar-laminated with millimetre scale alternations in grainsize	Wind-blown deposits formed by the fall out of sediment from suspension
<b>Smwr</b>	Ripple-cross-laminated sandstone		Purple-grey, very-fine to coarse-grained sandstone, bimodal sorted, well rounded	Undulose to ripple-cross-laminations with millimetre scale alternations in grainsize and sporadic coarse-grained lenses	Migration of wind-blown ripple-scale bedforms, producing pinstripe laminae
<b>Smwb</b>	Undulose-bedded sandstone		Purple-brown, very-fine to fine-grained sandstone, well sorted, well-rounded	Undulose to planar laminations with millimetre scale alternations in grainsize	Wind-blown deposits formed by the deflation of dune-scale bedforms over damp substrates

(continued)







Table 1. *Continued*

Code	Name	Lithology & texture	Sedimentary structures	Interpretation
<b>Sm</b>	Structureless sandstone	 Purple-grey, fine-grained sandstone, well sorted, well-rounded	Structureless with sporadic soft sediment deformation	Suspension settling of wind-blown sediment in areas affected by surface water, followed by drying
<b>Sxb</b>	Planar cross-bedded sandstone	 Purple-brown, fine to medium-grained sandstone, moderate/well sorted, sub-rounded	Planar cross-bedding with normal grading, in single or multiple sets with sporadic clasts, mud draping and soft sediment deformation	Migration of straight-crested dune-scale bedforms and dune trains subaqueously under lower flow regime conditions with high sediment load
<b>Stxb</b>	Trough cross-bedded sandstone	 Purple-brown, very-fine to fine-grained sandstone, moderate/well sorted, sub-rounded	Trough cross-bedding with normal grading, in single or multiple sets	Migration of sinuous-crested dune-scale bedforms and dune trains subaqueously under lower flow regime conditions
<b>Slxb</b>	Low-angle cross-bedded sandstone	 Purple-grey, fine-grained sandstone, moderate/well sorted, sub-rounded	Low-angle cross-bedding in single or multiple lenticular sets with sporadic mud-draped foresets and soft sediment deformation	Lateral migration of macro-forms in lower flow regime conditions with high sediment load
<b>Spb</b>	Planar bedded sandstone	 Purple-brown, fine to medium-grained sandstone, moderate/well sorted, sub-rounded	Planar bedding with sporadic rip-up clasts	Sub-aqueous upper flow regime flat beds
<b>Spl</b>	Planar laminated sandstone	 Purple-brown, fine to medium-grained sandstone, moderate/well sorted, sub-rounded	Planar laminations with sporadic rip-up clasts and mottling	Sub-aqueous upper flow regime flat beds

*(continued)*



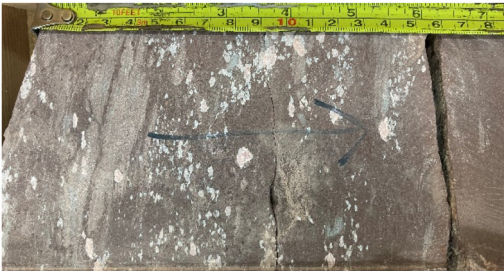





Table 1. Continued

Code	Name	Lithology & texture	Sedimentary structures	Interpretation
Sfr1	Ripple-cross-laminated sandstone	 Purple-brown, very-fine to fine-grained sandstone, moderate/well sorted, sub-rounded	Ripple-cross-laminations	Migration of ripple-scale bedforms in lower flow regime
Smf	Structureless sandstone	 Purple-brown-grey, fine to medium-grained sandstone, moderate/well sorted, sub-rounded	Structureless with sporadic rip-up clasts, evaporitic clasts and soft sediment deformation	Rapid deposition in high sediment load suppressing bedform development
Stpl	Planar laminated mudstone to siltstone	 Brown mudstone/siltstone	Planar laminations	Suspension fall-out from stationary waters
Cms	Matrix-supported conglomerate	 Brown-grey-purple, polymictic conglomerate with a fine to coarse-grained sandstone matrix and pebble to cobble-grade clasts, poorly sorted, sub-rounded, matrix supported	Structureless to planar bedded with sporadic rip-up clasts armoured with small extraformational granules and sporadic imbrication	Sub-aqueous lower flow regime conditions with high sediment load and suppressed bedform development
Ccs	Clast-supported conglomerate	 Brown-grey, polymictic conglomerate with pebble-grade clasts, poorly sorted, sub-angular to sub-rounded, clast supported	Structureless to planar bedded	Sub-aqueous, high energy Newtonian flow under high sediment load conditions, with suppressed bedform development
Ms	Structureless mudstone	 Brown mudstone	Structureless	Suspension fall-out in stationary waters


(continued)

Table 1. *Continued*

Code	Name	Lithology & texture	Sedimentary structures	Interpretation
<b>Sul</b>	Structured lake	 Brown, siltstone to fine-grained sandstone, moderate/poorly sorted, sub-rounded	Undulose lamination, sporadic coarser sandstone lenses, bioturbation, soft sediment deformation	Periodic sediment influx into stationary waters
<b>Seb</b>	Evaporitic bedded sandstone	 Purple-grey, very-fine to fine-grained sandstone, moderate/well sorted, sub-rounded	Crude bedding, sporadic evaporitic clasts, soft sediment deformation and bioturbation	Periodic sediment influx into saline stationary waters and subsequent precipitation of evaporites
<b>Steul</b>	Silty evaporitic structured lake	 Purple-brown, mudstone to fine-grained sandstone, moderate sorting, sub-rounded	Undulose to planar-bedding, coarser sandstone lenses, sporadic evaporitic clasts, bioturbation and soft sediment deformation	Periodic sediment influx into saline stationary waters and subsequent precipitation of evaporites
<b>Sml</b>	Structureless sandstone	 Grey, fine to medium-grained sandstone, well sorted, sub-rounded	Structureless, sporadic red diagenetic spots and soft sediment deformation	Rapid suspension fall-out from high density sediment influxes
<b>Spbl</b>	Planar-bedded sandstone	 Grey, fine-grained sandstone, well sorted, sub-rounded	Planar bedding, sporadic soft sediment deformation and coarser sandstone lenses	Periodic suspension fall-out in stationary waters
<b>Spil</b>	Planar-laminated siltstone	 Brown-grey, siltstone to very-fine-grained sandstone, bimodal sorting, sub-rounded	Planar laminations with polygonal hummocks, sporadic bioturbation	Sediment binding by algal and microbial mats with laminations indicating shallow water to subaerial exposure

*(continued)*

Table 1. Continued

Code	Name	Lithology & texture	Sedimentary structures	Interpretation	
<b>Sxl</b>	Cross-laminated sandstone		Purple-brown-grey siltstone to fine-grained sandstone, moderate sorting, sub-rounded	Cross-laminations to cross-bedding	Sub-aqueous formation and migration of ripple-scale bedforms

**Smbx**, Sub aerial planar cross-bedded sandstone; **Smbxc**, Sub aerial planar cross-bedded sandstone couplets; **Smtxb**, Sub aerial trough cross-bedded sandstone; **Smpb**, Sub aerial planar bedded sandstone; **Smpl**, Sub aerial planar laminated sandstone; **Smwr**, Sub aerial ripple-cross-laminated sandstone; **Smwb**, Sub aerial undulose laminated sandstone; **Sm**, Sub aerial structureless sandstone; **Sxb**, Sub aqueous planar cross-bedded sandstone; **Stxb**, Sub aqueous trough cross-bedded sandstone; **Slxb**, Sub aqueous low-angle cross-bedded sandstone; **Spb**, Sub aqueous planar bedded sandstone; **Spl**, Sub aqueous parallel laminated sandstone; **Sfrl**, Sub aqueous cross-laminated sandstone; **Smf**, Sub aqueous structureless sandstone; **Stpl**, Sub aqueous planar laminated mudstone/siltstone; **Cms**, Sub aqueous matrix-supported conglomerate; **Ccs**, Sub aqueous clast-supported conglomerate; **Ms**, Sub aqueous structureless mudstone; **Sul**, Sub aqueous undulose bedded sandstone; **Seb**, Sub aqueous evaporitic bedded sandstone; **Steul**, Sub aqueous evaporitic siltstone; **Sml**, Sub aqueous structureless sandstone; **Spbl**, Sub aqueous planar bedded sandstone; **Spil**, Sub aqueous planar laminated siltstone; **Sxl**, Sub aqueous cross-laminated sandstone.

plinth, aeolian sandsheet, dry interdune, damp to wet interdune, fluvial channel, fluvial sheet, overbank, lake margin, lake centre, and ephemeral saline lake/mudflat. The associations relate to 3 broad depositional environments: aeolian, fluvial and lacustrine, and 3 transition zones between the depositional environments: aeolian–fluvial, aeolian–lacustrine, and fluvial–lacustrine.

**Aeolian depositional environment**

Aeolian strata form the vast majority of the Lemna Sandstone and comprise the facies associations: aeolian dunes (AD), aeolian dune plinth (ADP), aeolian sandsheets (AS), dry interdunes (DI), damp to

wet interdunes (WI). Aeolian deposition is concentrated within the SE of the study area, particularly the eastern edge of quadrant 48 and western edge of quadrant 49, where aeolian dune and aeolian dune plinth associations dominate the depositional environment. Aeolian dunes (AD) range in thickness from 0.2 to 13 m and are characterized by centimetre-scale cross-bedded sandstones arranged into sets and cosets, with reverse graded foresets (Smbx/Smtxb) and sporadic ripple-cross-laminated sandstones (Smwr). In approximately 35–40% of occurrences the reverse graded foresets are separated by thin millimetre-scale finer grained laminae (Smbxc). Aeolian dune plinth associations (ADP) range in thickness from 0.2 to 7.5 m and are characterized by millimetre to centimetre-scale cross-laminated,

Table 2. Summary of facies associations with brief compositional description, along with their contained facies (see Table 1 for detailed facies descriptions), and thickness variations

Association	Code	Facies	Description
<b>Aeolian dune</b>	AD	Smbx, Smtxb, Smbxc, Smwr	Fine to coarse-grained sandstones arranged in sets of centimetre-scale cross-bedding of grainfall and grainflow strata, with sporadic ripple-cross-laminated sandstones. Association thickness ranges from 0.2–13 m.
<b>Aeolian dune plinth</b>	ADP	Smbxc, Smwr, Smpl	Bimodally sorted, very fine to coarse-grained sandstones with millimetre to centimetre-scale cross-laminated foresets to planar-laminated beds. Association thickness ranges from 0.2–7.5 m.
<b>Aeolian sandsheet</b>	AS	Smpb, Smpl	Very fine to medium-grained sandstones with millimetre to centimetre-scale planar laminations to bedding. Association thickness ranges from 0.25–5 m.
<b>Dry interdune</b>	DI	Smwr, Smpb, Smpl	Bimodally sorted, very fine to coarse-grained sandstones with millimetre to centimetre-scale planar to undulose laminations to bedding. Association thickness ranges from 0.2–2 m.
<b>Damp/wet interdune</b>	WI	Smwb, Sm, Ms	Very fine to fine-grained sandstones with either no structure or millimetre to centimetre-scale undulose laminations. Association thickness ranges from 0.15–2 m.
<b>Fluvial channel</b>	FC	Cms, Ccs, Sxb, Stxb, Smf, Spl, Spb, Sfrl	Erosional based fining upwards succession of pebble-grade conglomerates, to fine to medium-grained sandstones with cross-bedding and planar laminations, through to very fine to fine-grained ripple-cross-laminated sandstones. Association thickness ranges from 0.1–4.5 m.
<b>Fluvial sheet</b>	FS	Cms, Smf, Slxb, Spb, Spl, Sfrl	Fining upwards succession of matrix-supported, pebble-grade conglomerates, to fine to medium-grained structureless and low-angle to planar bedded sandstones, through to very fine to fine-grained ripple-cross-laminated sandstones. Association thickness ranges from 0.2–3.5 m.
<b>Overbank</b>	OB	Ms, Stpl	Structureless to parallel-laminated mudstones and siltstones. Association thickness ranges from 0.2–4 m.
<b>Lake margin</b>	LM	Sul, Spbl, Sxl	Siltstones to fine-grained sandstones with planar to undulose bedding and cross-laminations. Soft sediment deformation and bioturbation are common. Association thickness ranges from 0.2–6.75 m.
<b>Lake centre</b>	LC	Sml, Ms	Structureless to crudely laminated/bedded mudstones to fine-grained sandstones. Association thickness ranges from 0.15–7.5 m.
<b>Ephemeral saline lake/mudflat</b>	ESM	Spil, Steul, Seb	Mudstones to fine-grained sandstones with crudely undulose laminations and bedding. Coarser-grained lenses, soft sediment deformation, bioturbation and evaporitic clasts are common. Association thickness ranges from 0.5–19.5 m.



bimodally sorted sandstones (Smwr). Several areas of aeolian deposition are also distributed between areas of dominantly fluvial deposition in the centre of quadrant 48 and comprise predominantly aeolian sandsheet associations with minor aeolian interdune associations and less extensive aeolian dune associations. The aeolian sandsheets (AS) range in thickness from 0.25 to 5 m and are characterized by millimetre to centimetre-scale planar-bedded to laminated sandstones (Smpb/Smpl) with sporadic granule-rich bounding surfaces. Aeolian interdune associations have been divided into dry and damp to wet interdunes. The dry interdunes (DI) range in thickness from 0.2 to 2 m and are characterized by millimetre to centimetre-scale planar-bedded to laminated sandstones (Smpb/Smpl) and cross-laminated, bimodally sorted sandstones (Smwr), whereas the damp to wet interdunes (WI) range in thickness from 0.15 to 2 m and are characterized by millimetre to centimetre-scale undulose laminated sandstones (Smwb) and structureless mudstones (Ms) to fine-grained sandstones (Sm).

The aeolian depositional environment comprises predominantly well-developed, straight to sinuous-crested transverse dunes which decrease in size and become more isolated towards the fluvial corridor and lacustrine margin. Sets and cosets of reverse graded foresets represent the deposits of individual grainflow avalanches, with the finer-grained laminae between the grainflows representing grainfall strata (Hunter 1977a, b; Langford and Chan 1989; Kocurek 1991, 1996). The absence of the grainfall between individual grainflow avalanches may indicate deposition in the upper parts of the dune slipfaces of substantially sized dunes (Besly *et al.* 2018). Occurrences of the bimodally sorted, cross-laminated sandstones represent wind-ripple strata climbing up the dune toe from associated dune plinth associations, however thick units of the wind-ripple strata possibly indicate that some duneforms may have a linear geomorphology (Besly *et al.* 2018). The aeolian sandsheet associations and interdunes form where dune development is inhibited (*cf.* Kocurek and Nielson 1986), in this case, as a result of episodic flooding (Kocurek and Nielson 1986) and/or a high water table which is in contact with sediment surface (Fryberger *et al.* 1988; Jagger 2003; Mountney and Jagger 2004), which is especially prominent within the transition zones between the aeolian and fluvial/lacustrine environments. The granule-rich bounding surfaces within planar-bedded sandstones of the aeolian sandsheets, represents deflationary surfaces, characteristic of sandsheet development (Langford and Chan 1989).

### Fluvial depositional environment

Fluvial strata are more prevalent within a SE–NW transect through the centre of quadrant 48, forming a fluvial corridor through the aeolian dune field. The facies associations identified are fluvial channels (FC), fluvial sheets (FS), and overbank (OB). Fluvial channels and sheets dominate the association with minimal overbank preserved. The channels (FC) within the fluvial corridor are typically stacked and amalgamated with minor matrix to clast-supported conglomeratic bases (Cms/Ccs). They typically display a progressively upwards fining fill, and range in thickness from 0.1 to 4.5 m. Isolated channels are also observed between the deposits of aeolian dune, and distally feeding into the desert lake. Cross-bedded sandstones (Sxb) and structureless sandstones (Smf) form most of the channel fill, with planar-bedded to laminated sandstones (Spb/Spl) and ripple-cross-laminated sandstones (Sfrl) forming the upper units of the fining upwards succession. The fluvial sheets (FS) are more abundant within the distal reaches of the fluvial corridor, towards the desert lake. They are characterized by a fining upwards succession but display little to no downcutting erosion along the basal bounding surface, and range in thickness from 0.2 to 3.5 m. Planar-bedded to laminated sandstones (Spb/Spl) and low-angle cross-bedded sandstones (Slxb) dominant the succession, with sporadic

matrix-supported clasts (Cms) along the basal surface and very-fine to fine-grained ripple-cross-laminated sandstones (Sfrl) towards the top of the succession. The sporadic overbank associations range in thickness from 0.2 to 4 m and are characterized by structureless mudstone (Ms) and parallel-laminated mudstones to siltstones (Stpl) and exhibit sporadic rhizoliths, desiccation cracks and bioturbation.

The fluvial depositional environment comprises channels associated with rapid deposition from high-energy currents and sheets associated with unconfined flow during flash-flood events or possibly in relation to flooding from breaks in channel walls (*cf.* Abdullatif 1989; Sadler and Kelly 1993; Tooth 1999, 2000, 2005; Billi 2007; Sáez *et al.* 2007; Moscariello 2011), deposited in an ephemeral fluvial system in a semi-arid desert environment (Moscariello 2011). The conglomeratic basal units of the fluvial channels represent lag deposits formed with high flow velocities, and as the flow waned, sets of cross-bedding were deposited and represent the migration of dune-scale bedform trains along the bases of channels during times of lower sediment load. Planar-laminated and planar-bedded sandstones near the top of the association represent upper flow regime deposits produced as a result of rapidly decreasing flow depth. The presence of low-angle cross-bedding interspersed with planar-bedding within the fluvial sheets represents the transition from conditions of lower flow regime dune formation to upper flow regime plane bed formation, probably formed under high rates of sediment deposition (Fielding 2006; Lang and Winsemann 2013). The abundance of planar-bedded and planar-laminated sandstones suggest upper flow regime conditions dominated (Arnott and Hand 1989; Carling 2013; Guan *et al.* 2016). Whereas the ripple-cross-laminated sandstones towards the top of the association suggest flow waned enough for bedform development and migration. The overbank associations indicate deposition from suspension settling in standing water after flooding (Eberth and Miall 1991), where discharge temporarily exceeded the bank-full capacity of the local channel network (*cf.* Bridge 1984, 2003; Bristow *et al.* 1999). Planar-laminations within the siltstones and mudstones represent minor grain-size differences resulting from the alternation of episodic discharge of sediment (Moscariello 2011), and the presence of desiccation cracks and rhizoliths indicate stabilization and drying of the floodplain (Miall 1988).

### Lacustrine depositional environment

Lacustrine strata form the vast majority of the Silverpit Formation and comprise the facies associations: lake margin (LM), lake centre (LC), and ephemeral saline lake/mudflat (ESM). Lacustrine deposition is concentrated in the NE of the study area, particularly northern region of quadrants 48 and 49. The lake margin (LM) association ranges in thickness from 0.2 to 6.75 m and is characterized by centimetre-scale planar to undulose bedded siltstones and sandstones (Spbl/Sul) and millimetre-scale cross-laminated sandstones (Sxl) with sporadic mud-draping along foresets. Soft sediment deformation, fluid escape structures and bioturbation are all common features within the association. The lake centre (LC) association ranges in thickness from 0.15 to 7.5 m and is characterized by structureless to crudely bedded mudstones (Ms), siltstones and sandstones (Sml). During more arid times, the ephemeral saline lake/mudflat (ESM) forms the outskirts of the Silverpit desert lake and ranges in thickness from 0.5 to 19.5 m. The association is characterized by millimetre to centimetre-scale crudely undulose laminated mudstones to fine-grained sandstones (Stpl/Seb), along with parallel-laminated siltstones to very-fine sandstones (Spll). The crudely undulose laminated mudstones to fine-grained sandstones (Stpl/Seb) contain sporadic coarser grained lenses with internal planar-laminations, evaporitic clasts up to 7 cm in diameter, soft sediment deformation and bioturbation, whereas the parallel-laminated siltstones to very-fine sandstones (Spll) have sporadic polygonal hummocks and bioturbation.

The Silverpit desert lake exhibits the expansion and contraction of a lacustrine environment during intermittent more humid and more arid conditions. The ephemeral saline lake/mudflat association formed during the evaporation and desiccation of previously more established lakes (*cf.* Pettigrew *et al.* 2020, 2021). Parallel laminations of alternating siltstones and sandstones with polygonal hummocks result from sediment binding by algal and microbial mats with laminations indicating shallow water to subaerial exposure (Van Dover 2000; Reitner 2011; McKay *et al.* 2016; Pettigrew *et al.* 2020, 2021), and the crudely undulose laminated to bedded mudstones to sandstones with sporadic evaporitic clasts result from periodic sediment influx into saline stationary waters where variations in ground water levels and circulation promoted subsurface phreatic evaporite growth as random crystals or nodules (Smoot and Lowenstein 1991; Warren 2006; Boggs and Boggs 2009; Pettigrew *et al.* 2020, 2021). The lake margin and lake centre associations formed during more humid times, where the lake was more established. The fine-grained nature of the associations suggests a predominantly low-energy environment, with deposition occurring within a standing body of water, while the undulose sandstone and siltstone laminae reflect periods of increased energy resulting from episodic discharge of sediment into the standing body of water (Moscariello 2011; Andrews and Hartley 2015). Cross-laminated siltstones to sandstones within the lake margin resulted from the subaqueous formation and migration of ripple-scale bedforms, possibly influenced by current circulation as a result of prevailing winds, indicating periods of high water table but shallow water depths (Allen 1963; Nielsen 1981).

## Petrophysics

Log derived gamma ray, sonic, bulk density and neutron porosity data have been analysed for each well and combined into the three broad depositional environments of aeolian, fluvial and lacustrine, and three transition zones between the depositional environments of aeolian–fluvial, aeolian–lacustrine, and fluvial–lacustrine. For each of the petrophysical datasets, the mean, median, interquartile range, minimum and maximum measurements and standard deviations have been calculated and summarized in Table 3.

### Gamma ray

The sediments of the aeolian, aeolian–fluvial and aeolian–lacustrine environments exhibit the lowest gamma ray response, with the sediments of the aeolian environment ranging from 29.7 to 40.7 API, the sediments of the aeolian–fluvial environment ranging from 27.6 to 39.0 API and the sediments of the aeolian–lacustrine environment ranging from 25.4 to 44.8 API (Table 3; Fig. 6). The sediments of the aeolian and fluvial environments have the lowest mean gamma ray response (35.2 & 35.1 API, respectively), followed by the sediments of the aeolian–lacustrine (38.8 API), however, contrary to the mean values, the sediments of the aeolian–lacustrine environment have the lowest median gamma ray response (30.4 API), followed by the sediments of the aeolian–fluvial and aeolian environments (32.9 & 36.0 API, respectively). The sediments of the fluvial environment have a slightly higher gamma ray response, ranging from 34.5 to 54.6 API, with a

**Table 3.** Summary of the wireline data for each depositional environment and transitional environments, including the interquartile range, minimum, maximum, median, mean and standard deviation for gamma ray, sonic, bulk density and neutron porosity measurements

Environment	Gamma ray response (API)	Sonic transit time ( $\mu\text{s}/\text{ft}$ )	Bulk density ( $\text{g cm}^{-3}$ )	Neutron porosity (%)
Aeolian	Range: 29.7–40.7 Min: 14.8 Max: 57.3 Median: 36.0 Mean: 35.2 SD: 7.63	Range: 70.8–78.6 Min: 48.8 Max: 108.5 Median: 74.7 Mean: 74.8 SD: 5.85	Range: 2.38–2.48 Min: 2.09 Max: 2.66 Median: 2.43 Mean: 2.43 SD: 0.07	Range: 9.11–14.1 Min: 1.96 Max: 23.9 Median: 11.5 Mean: 11.5 SD: 3.50
Fluvial	Range: 34.5–54.6 Min: 25.3 Max: 142.9 Median: 39.8 Mean: 48.9 SD: 23.0	Range: 65.6–72.9 Min: 60.3 Max: 83.9 Median: 69.3 Mean: 69.9 SD: 5.16	Range: 2.45–2.58 Min: 2.27 Max: 2.73 Median: 2.50 Mean: 2.51 SD: 0.09	Range: 3.57–11.9 Min: 0.75 Max: 18.0 Median: 7.75 Mean: 8.11 SD: 4.94
Lacustrine	Range: 77.9–104.7 Min: 33.5 Max: 144.9 Median: 92.5 Mean: 90.7 SD: 19.2	Range: 61.4–65.1 Min: 54.6 Max: 76.3 Median: 63.2 Mean: 63.4 SD: 3.10	Range: 2.62–2.68 Min: 1.70 Max: 2.74 Median: 2.66 Mean: 2.60 SD: 0.16	Range: 10.1–14.2 Min: 2.21 Max: 35.0 Median: 12.1 Mean: 12.6 SD: 3.96
Aeolian–fluvial	Range: 27.6–39.0 Min: 18.4 Max: 122.4 Median: 32.9 Mean: 35.1 SD: 12.0	Range: 63.7–72.2 Min: 55.8 Max: 92.8 Median: 68.7 Mean: 69.0 SD: 6.99	Range: 2.46–2.59 Min: 2.13 Max: 2.73 Median: 2.51 Mean: 2.51 SD: 0.11	Range: 4.52–9.19 Min: 1.66 Max: 17.6 Median: 7.11 Mean: 7.15 SD: 3.08
Aeolian–lacustrine	Range: 25.4–44.8 Min: 15.8 Max: 120.2 Median: 30.4 Mean: 38.8 SD: 20.8	Range: 63.4–73.3 Min: 53.6 Max: 96.4 Median: 67.3 Mean: 68.3 SD: 6.81	Range: 2.51–2.60 Min: 2.31 Max: 2.73 Median: 2.55 Mean: 2.55 SD: 0.06	Range: 8.56–11.6 Min: 0.75 Max: 22.9 Median: 10.0 Mean: 10.2 SD: 2.88
Fluvial–Lacustrine	Range: 41.5–82.9 Min: 22.3 Max: 139.4 Median: 57.0 Mean: 63.0 SD: 25.5	Range: 64.7–68.8 Min: 59.7 Max: 82.3 Median: 66.6 Mean: 67.3 SD: 3.97	Range: 2.54–2.66 Min: 2.29 Max: 2.76 Median: 2.60 Mean: 2.60 SD: 0.08	Range: 11.0–14.4 Min: 7.52 Max: 23.2 Median: 12.3 Mean: 12.9 SD: 2.80

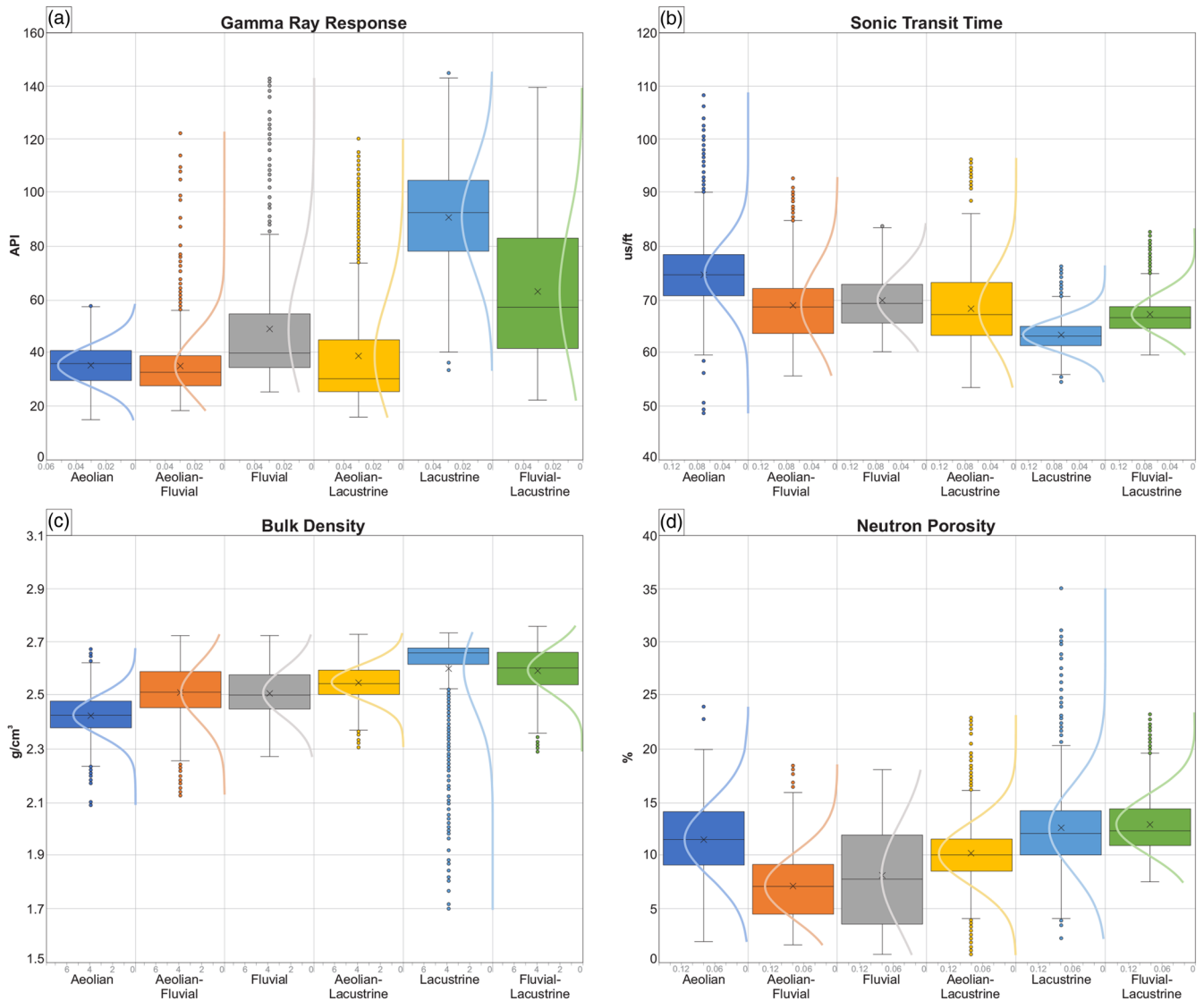


**Fig. 6.** Box and whisker plots for each depositional environment and transitional environment of (a) gamma ray, (b) sonic, (c) bulk density and (d) neutron porosity. Each plot is overlain by a normal distribution curve highlighting the standard deviation of the datasets.

median value of 39.8 API and mean value of 48.9 API (Table 3; Fig. 6). The sediments of the fluvial environment also exhibit a broad range of outliers within the dataset, with a maximum gamma ray response of 142.9 API (Table 3; Fig. 6). A similar abundance of outliers within the dataset are also observed in the sediments of the aeolian–fluvial and aeolian–lacustrine environments, with maximum gamma ray responses of 122.4 API and 120.2 API, respectively. As expected, the sediments of the lacustrine environment have the highest gamma ray response (range: 77.9–104.7 API, median: 92.5 API), followed by the sediments of the fluvial–lacustrine environment (range: 41.5–82.9 API, median: 57.0 API) (Table 3; Fig. 6).

The lower gamma ray responses of the aeolian–lacustrine and aeolian–fluvial sediments are interpreted as the product of extensive recycling of the sediment within the environments, ultimately producing a cleaner, quartz-rich sandstone. Whereas the highest gamma ray responses observed in the sediments of the lacustrine and fluvial–lacustrine environments are due to the amount of siltstone and mudstone within these depositional systems. The broad range of gamma ray responses within the sediments of the fluvial, aeolian–fluvial, and aeolian–lacustrine environments represents the variance in lithology within the facies associations within these depositional environments.

### Sonic

The sediments of the lacustrine and fluvial–lacustrine environments have the quickest sonic transit times, with the lacustrine sediments median acoustic slowness of 63.2  $\mu\text{s}/\text{ft}$  and interquartile range from 61.4 to 65.1  $\mu\text{s}/\text{ft}$ , and the fluvial–lacustrine sediments median acoustic slowness of 66.6  $\mu\text{s}/\text{ft}$  and interquartile range from 64.7 to 68.8  $\mu\text{s}/\text{ft}$  (Table 3; Fig. 6). The sediments of the aeolian environment have the slowest sonic transit times, ranging from 70.8 to 78.6  $\mu\text{s}/\text{ft}$ , with a median acoustic slowness of 74.7  $\mu\text{s}/\text{ft}$ . The aeolian sediments also exhibit the largest range of outliers within the dataset, with a quickest sonic transit time of 48.8  $\mu\text{s}/\text{ft}$  and a slowest sonic transit time of 108.5  $\mu\text{s}/\text{ft}$  (Table 3; Fig. 6). The sediments of the fluvial, aeolian–fluvial, and aeolian–lacustrine environments all exhibit similar median sonic transit times and ranges (69.3 & 65.6–72.9  $\mu\text{s}/\text{ft}$ ; 68.7 & 63.7–72.2  $\mu\text{s}/\text{ft}$ ; 67.3 & 63.4–73.3  $\mu\text{s}/\text{ft}$ , respectively).

The slow sonic transit times observed in the sediments of the aeolian environment represent longer acoustic travel times as a result of high porosity. The broad range of outliers within the aeolian sediments represent the large variation in facies, with the clean, quartz-rich, well-sorted sandstones, dominated by grainflow facies of the aeolian dune facies association represented by the

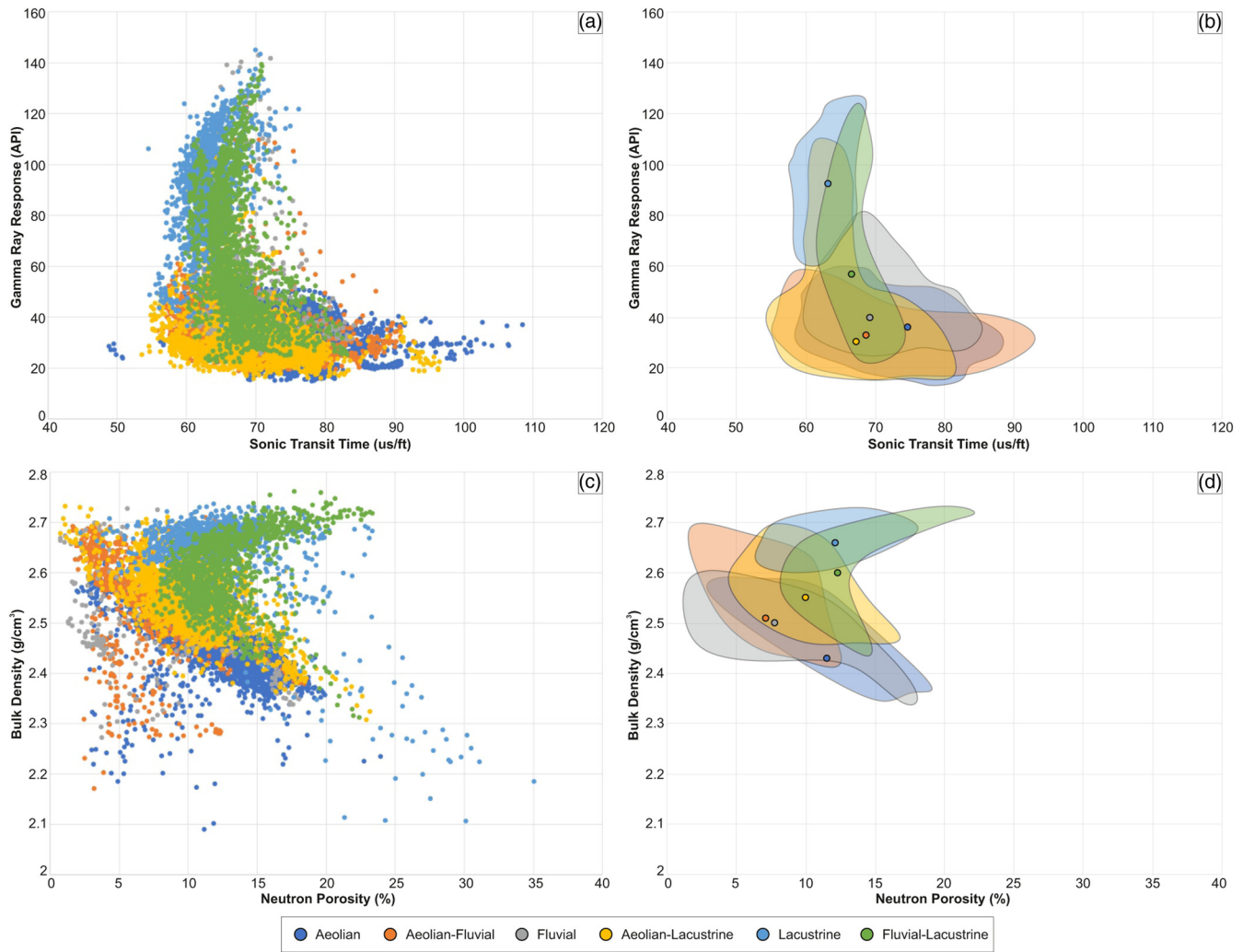


**Fig. 7.** Cross plots of (a) gamma ray v. sonic (all values), (b) gamma ray v. sonic (median values (dots) and interquartile range clusters), (c) bulk density v. neutron porosity (all values), (d) bulk density v. neutron porosity (median values (dots) and interquartile range clusters).

slower sonic transit times and small interdunes represented by the quicker sonic transit times. Internal variations within the dune facies associations, such as couplets of lower porosity grainfall and higher porosity grainflow facies, along with the bimodally sorted wind-ripple facies, will also contribute to the array of sonic transit times observed. The quicker sonic transit times observed in the sediments of the lacustrine and fluvial-lacustrine environments are due to the amount of lower porosity siltstone and mudstone within these depositional systems.

### Bulk density

The sediments of the aeolian environment have the lowest bulk density values, ranging from 2.38 to 2.48 g cm<sup>-3</sup>, with a median bulk density of 2.43 g cm<sup>-3</sup> (Table 3; Fig. 6). Whereas, the sediments of the lacustrine and fluvial-lacustrine environments have the highest bulk density values, with the lacustrine sediments median bulk density of 2.66 g cm<sup>-3</sup> and interquartile range from 2.62 to 2.68 g cm<sup>-3</sup>, and the fluvial-lacustrine sediments median bulk density of 2.60 g cm<sup>-3</sup>, and interquartile range from 2.54 to 2.66 g cm<sup>-3</sup> (Table 3; Fig. 6). The lacustrine sediments also exhibit the broadest range of outliers within the dataset, with a minimum bulk density of 1.70 g cm<sup>-3</sup>. The sediments of the fluvial, aeolian-fluvial, and aeolian-lacustrine environments all exhibit similar median bulk densities and ranges (2.50 & 2.45–2.58 g cm<sup>-3</sup>; 2.51 & 2.46–2.59 g cm<sup>-3</sup>; 2.55 & 2.51–2.60 g cm<sup>-3</sup>, respectively) (Table 3; Fig. 6).

The majority of the bulk density measurements fall between the range of 2.4–2.6 g cm<sup>-3</sup>, indicating the presence of sandstones and siltstones. The similar measurements are attributed to the extensive recycling of the sediments within the depositional environments. The sediments of the lacustrine and fluvial-lacustrine environments have slightly higher bulk density measurements due to the presence of more siltstones/mudstones, with the highest bulk densities in the lacustrine sediments due to the presence of evaporitic nodules. The abundance of outliers within the lacustrine sediments also depicts the varying lithologies present, with the lowest bulk density of 1.70 g cm<sup>-3</sup> potentially representing the presence more organic-rich mudstones.

### Neutron porosity

Contrary to conventional observations, sediments of the fluvial and aeolian-fluvial environments have the lowest neutron porosity values, and the sediments of the lacustrine, fluvial-lacustrine environments have the highest neutron porosities, along with the expected aeolian sediments (Table 3; Fig. 6). The sediments of the fluvial environment have a median neutron porosity value of 7.75%, and an interquartile range of 3.57–11.9%, and the sediments of the aeolian-fluvial environment have a median neutron porosity value of 7.11%, and an interquartile range of 4.52–9.19% (Table 3; Fig. 6). The sediments of the fluvial-lacustrine environment have the highest median neutron porosity value of 12.3%, and an interquartile range of 11.0–14.4%, with the lacustrine sediments



exhibiting the second highest median neutron porosity value of 12.1%, and an interquartile range of 10.1–14.2%. The lacustrine sediments also have the broadest range of outliers within the dataset, with a minimum neutron porosity of 2.21% and a maximum neutron porosity of 35.0% (Table 3; Fig. 6). The neutron porosity of the aeolian sediments have an interquartile range from 9.11 to 14.1%, with a median neutron porosity of 11.5%, and a maximum neutron porosity of 23.9%. The sediments of the aeolian–lacustrine environment also exhibit a broad range of outliers within the dataset, with a minimum neutron porosity of 0.75%, a maximum neutron porosity of 22.9%, an interquartile range of 8.56–11.6%, and a median neutron porosity of 10.0% (Table 3; Fig. 6).

The lower neutron porosity values within sediments of the fluvial and aeolian–fluvial environments are interpreted to be the result of cemented gravel lags and mudstone lenses within the fluvial channels and sheets. The highest neutron porosity values were observed within the sediments of the fluvial–lacustrine and lacustrine environments, this could be due to water within the mudstone composition, therefore resulting in high hydrogen measurements usually associated with higher neutron porosities. The broad range of neutron porosities observed within the sediments of the lacustrine environment is also due to the complex composition of the deposits, ranging from claystones to fine-grained sandstones and evaporites to carbonates. The relatively high neutron porosities within the sediments of the aeolian environment are a result of the mature, well-rounded and well-sorted sandstones.

### Cross-plots

Cross-plots of gamma ray v. sonic and bulk density v. neutron porosity have been produced to identify clusters within the dataset representing the sediments of each depositional environment (Fig. 7). The gamma ray v. sonic cross-plot displays large overlap between the deposits of the aeolian, aeolian–fluvial, fluvial and aeolian–lacustrine environments, clustering around 20 to 60 API and 55 to 90  $\mu\text{s}/\text{ft}$  (Fig. 7a, b). Whereas the sediments of the lacustrine and fluvial–lacustrine environments cluster around 40 to 125 API and 60 to 70  $\mu\text{s}/\text{ft}$  (Fig. 7a, b).

The bulk density v. neutron porosity cross plot again shows a considerable amount of overlap between the sediments of the depositional environments, particularly the aeolian and fluvial deposits, clustering around 2 to 18% and 2.35 to 2.6  $\text{g cm}^{-3}$  (Fig. 7c, d). The sediments of the aeolian–fluvial and aeolian–lacustrine environments also show a similar clustering pattern, separated by a 2–3% difference in porosity (Fig. 7c, d). The sediments of the fluvial–lacustrine environment have a broad ‘C’ shape cluster, indicating higher porosities around 2.7 and 2.45  $\text{g cm}^{-3}$  (Fig. 7c, d).

The large overlap between the deposits of the aeolian, aeolian–fluvial, fluvial and aeolian–lacustrine environments in the cross-plots is considered to be the result of the extensive sediment recycling between the depositional environments, producing well-sorted, well-rounded sandstones of high reservoir quality. This is particularly evident within the deposits of the coeval aeolian and fluvial environments, with the wind-blown sediments transported by saltation into the neighbouring fluvial channels and by the cannibalisation on the aeolian deposits by the migration and/or expansion of the fluvial system (Priddy and Clarke 2020; Priddy 2021). The aeolian sediment within the fluvial system then gets reworked within the flow and ultimately deposited within the shoreline of the lacustrine environment. Similar to the deposits of the aeolian–fluvial environment, the wind-blown sediments can also be transported by saltation into the shoreline of lake. Recycling of the fluvial and lacustrine sediments by the aeolian system can also occur. As the flow wanes within the fluvial environment and both the

fluvial and lacustrine environments dry out, the sediment became available for wind-blown transportation and ultimately recycled into aeolian duneforms (Priddy and Clarke 2020; Priddy 2021).

### Facies maps

Facies maps have been created by correlating and extrapolating data from the 19 cored wells. Several cycles of erg transgression/lacustrine regression and lacustrine transgression/erg regression can be recognized throughout the expanse of the Leman Sandstone and Silverpit formations, which can be related to climatic cyclicity (George and Berry 1993; Howell and Mountney 1997). Expansion and contraction of the aeolian and lacustrine systems are also linked to the expansion and migration of the fluvial system.

Fluvial deposition is concentrated within quadrant 48 of the study area, acting as a fluvial corridor through the erg and ultimately feeding the desert lake. As the fluvial deposition diminishes, aeolian deposition takes over, where the aeolian deposits are initially dominated by sandsheet associations before the development of aeolian duneforms. Three to four cycles of fluvial deposition can be observed before the drying of the system and deposition of aeolian sediments. The last major fluvial deposition occurs approximately halfway through the Leman Sandstone due to the rejuvenation of the fluvial source terrain (Fig. 8a, models 4/5) (George and Berry 1993). From this point onwards aeolian deposition dominated within the proximal region, and lacustrine deposition dominated within distal region. Minor fluvial deposits are still observed between the deposits of aeolian dunes, as the fluvial system was funnelled through interdune corridors towards the desert lake (Fig. 8).

Aeolian deposition is concentrated in the eastern and western portions of the study area; either side of the fluvial corridor, with the preserved deposits of cross-bedded aeolian duneforms dominating the successions. The aeolian dune elements are composed of predominantly grainflow strata and couplets of grainfall/grainflow strata, suggesting the dune morphology was likely transverse. However, sporadic occurrences of thick units of inclined wind-ripple strata possibly indicate that some duneforms may have had a linear geomorphology.

Lacustrine deposition is concentrated to the north/northeastern region of the study area, however the deposits extend relatively far south, particularly within the eastern portion of the study area, where extensive, thick lacustrine deposits are observed halfway down the border between quadrant 48/49 (Fig. 8). The lacustrine sediments are predominantly sandy in composition due to the interaction with the aeolian system, preventing the carbonate development, however, during more arid conditions, the lake contracts and subsequent evaporites are precipitated within the lake margins. Cycles of lake expansion and contraction are also observed, with the fringes of the desert lake encroaching on the edge of the dune field (Fig. 8).

### Discussion

With recent UK government targets to reach ‘net zero’ by 2050, and to achieve the ambitious aims of reducing emissions and global warming below 1.5°C set out at in the Paris Agreement at COP21 (UN 2015), the UK government has recently published reports into the feasibility of CCS (OGUK 2021, 2022) and hydrogen storage (HM Government 2021). The first CCS license round began in June 2022 with 20 licenses offered for award by the NSTA in May 2023 with two awarded track 2 status at the time of writing – the Viking and Acorn CCS projects (Department for Energy Security & Net Zero 2023). The North Sea is in a unique position to be at the forefront of CCS due to the wealth of legacy open access data and subsurface knowledge of the area, combined with some of the

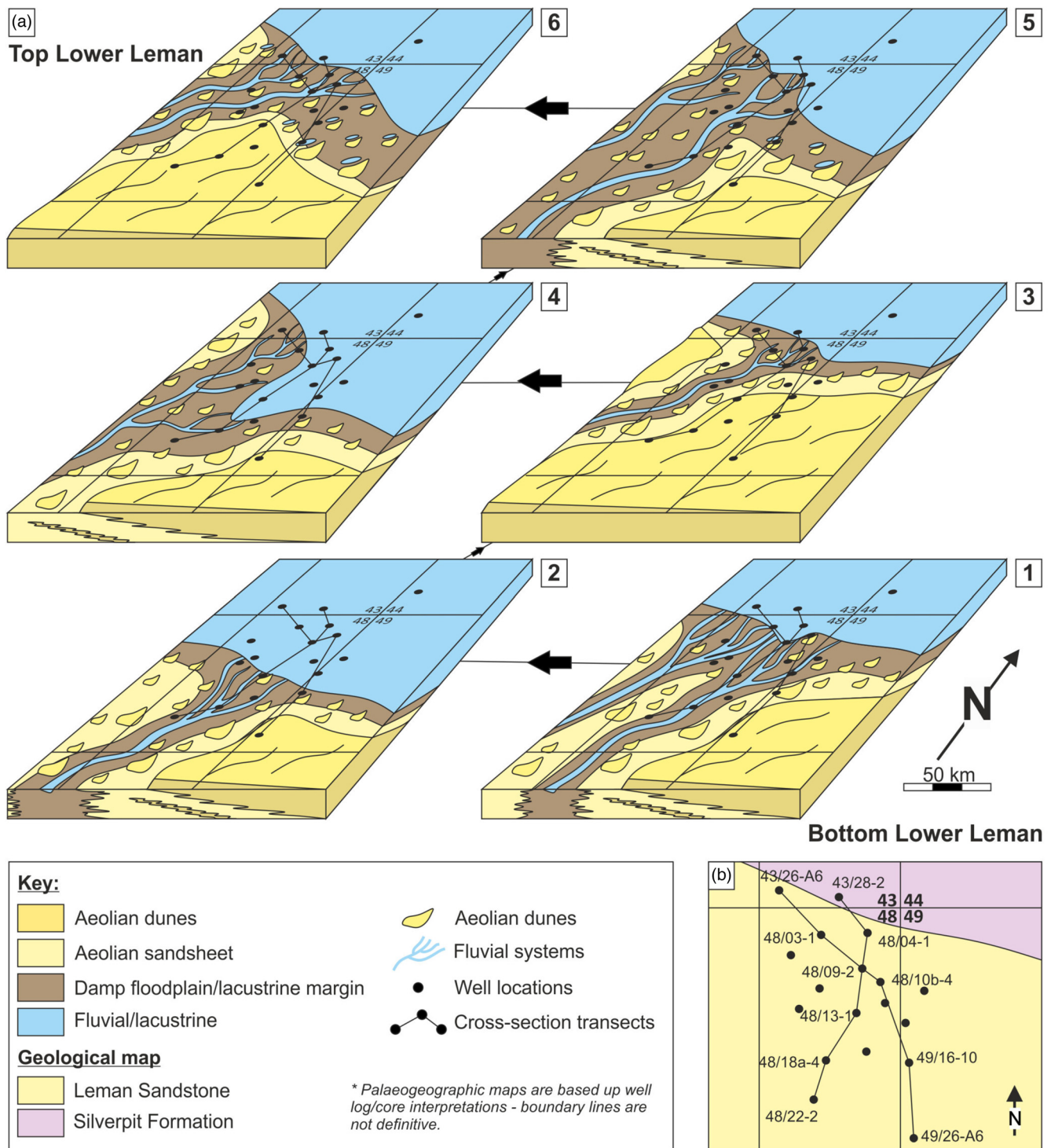


**Fig. 8.** Palaeogeographical maps through key time intervals of Leman Sandstone deposition, highlighting the expansion and contraction of the aeolian dune field and Silverpit lake, as well as the progradation, retrogradation, and migration of the Leman Sandstone fluvial system.

world’s best existing offshore infrastructure which could be repurposed into storage centres reducing the need for costly decommissioning (Underhill *et al.* 2023).

The availability of the NSTA data sets from the previous 60 years of hydrocarbon exploration has allowed for a more detailed and regional investigation of the erg-margin transition between the Leman Sandstone and Silverpit formations of the Southern North Sea Basin, previously not available when stakeholder or commercial limitations apply to individual license blocks or areas.

Previous work has focused on the hydrocarbon prospectivity and heterogeneities of the gas bearing aeolian units (Glennie *et al.* 1978; Arthur *et al.* 1986; Weber 1988; Hillier and Williams 1991),

however few studies have been conducted on the transitional zones between the central erg, fluvial corridor, and lake margin due to the complexities related to production within these units (George and Berry 1993; Howell and Mountney 1997; Sweet 1999). By combining legacy wireline data with sedimentological facies analysis of corresponding cored sections, and by focusing on the transitional zones between depositional environments rather than the potential prospectivity of hydrocarbon bearing units, a more detailed investigation of the complex sedimentary interactions and regional extents of the depositional environments has been conducted, resulting in an unbiased and regional interpretation from a wide scale holistic dataset.

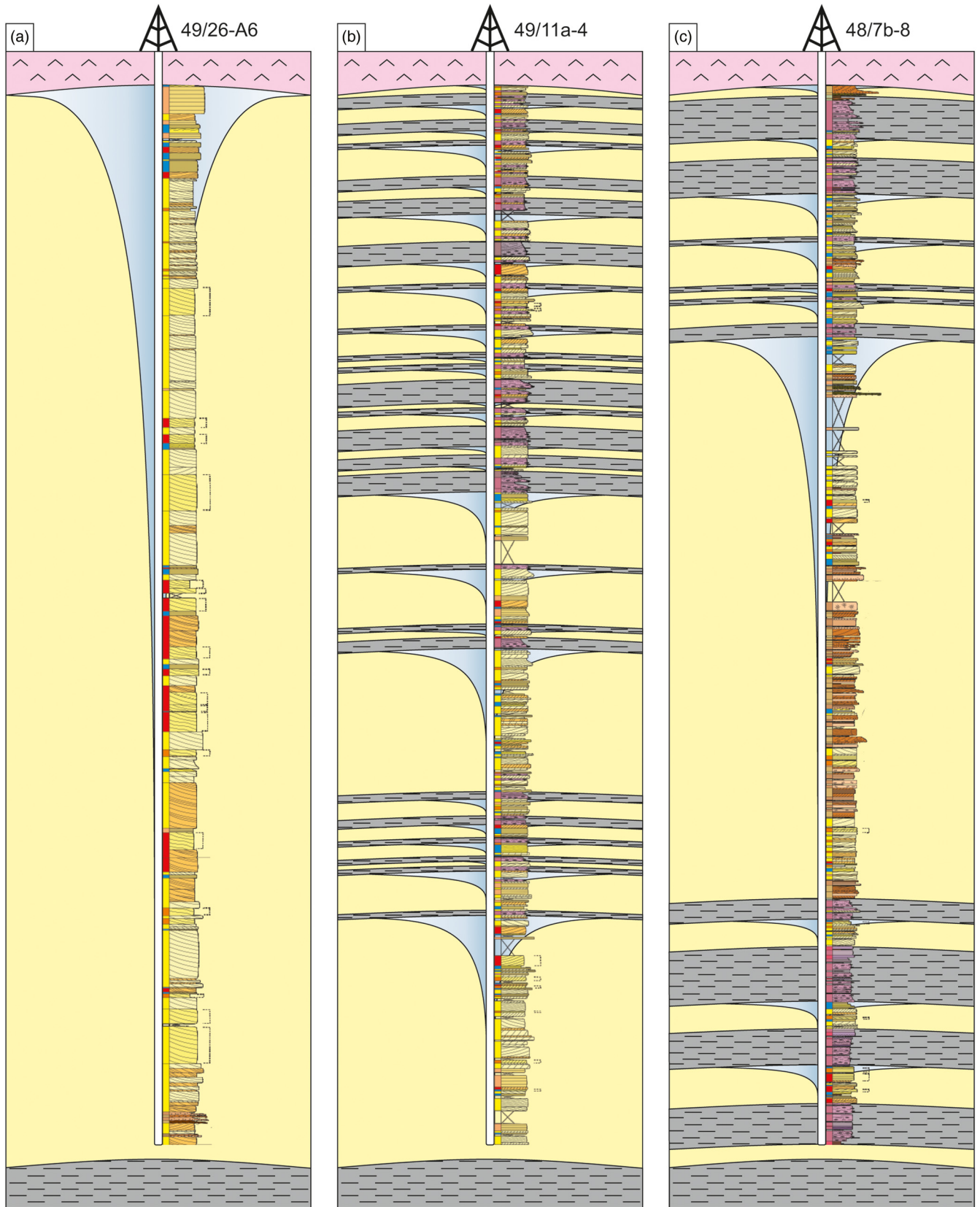


**Fig. 9.** Schematic diagrams of CO<sub>2</sub> plumes within different types of reservoirs using examples of three cored wells within the study area. (a) Well 49/26-A6 representing a homogeneous reservoir composed of aeolian dune sandstones, with a single CO<sub>2</sub> plume. (b) Well 49/11a-4 representing a heterogeneous reservoir, composed of mixed aeolian and lacustrine sediments, with multiple CO<sub>2</sub> plumes, increasing the surface area for CO<sub>2</sub> storage. (c) Well 48/7b-8 representing another heterogeneous reservoir, composed of mixed, aeolian, fluvial and lacustrine sediments, with multiple CO<sub>2</sub> plumes. (see Fig. 2 for detailed key for sedimentary logs).

## Sedimentological viability of the Leman Sandstone

This study utilized both sedimentological data from core and petrophysical data from well logs to analyse the sedimentary interactions between the erg-lacustrine margin of the Leman Sandstone. A total of 19 wells were investigated, including legacy wireline data for 11 wells from the NDR. In this case, the potential targeted CO<sub>2</sub> storage sites are located below the extensive salt deposits of the Zechstein Supergroup, in which seismic resolution is of poor quality. Wells with good core recovery, arranged in an approximate grid pattern allowing for down dip and across strike analysis of the depositional environments, were logged utilizing core from the BGS core store. This wealth of open-source data from multiple sources allows for regional interpretation and assessments to be conducted without the limitations of proprietary data and restrictions of hydrocarbon explores related to license rounds and blocks, and as a result, regional palaeogeographic maps were created.

George and Berry (1993) also recognized five distinct lithostratigraphic units within the Upper Rotliegend stratigraphy, relating to drying upwards cycles observed within the aeolian, fluvial and lacustrine depositional environments. Detailed regional scale palaeogeographic maps of each of the lithostratigraphic units were then reconstructed from well data illustrating the evolution of the Upper Rotliegend. The palaeogeographic maps from this work show similarities to those of George and Berry (1993) particularly with the expansion, contraction, and migration of the fluvial systems, however the work presented here suggested the palaeoshore of the Silverpit lake may have extended further south than previously interpreted.

While both of these palaeogeographical interpretations provide useful regional scale information of the sedimentary environments which can be used to further understand the extent of large-scale reservoir heterogeneities, intraformational seals and cyclic patterns caused by the expansion and contraction of the aeolian, fluvial and lacustrine depositional environments. It is the combined core and wireline analysis, along with cross plots of the petrophysical data for each depositional environment which has allowed for a more detailed analysis of the small-scale heterogeneities caused by facies scale sedimentary processes and sediment recycling.

The clean aeolian sandstones of the Leman Sandstone, initially targeted for hydrocarbon reservoirs, may not be the most effective reservoirs for CCS. Areas where there are multiple interactions between the aeolian dune field, and coeval environments, such as the erg-lacustrine margin could potentially be a more suitable target for CO<sub>2</sub> storage due to intraformational seals within the reservoir units formed by laterally extensive lacustrine mudstones deposited during the transgression of the lake into the aeolian dune field (Fig. 9). These areas are comparatively understudied within the Leman Sandstone when compared with the data collected for the purely aeolian environment. Therefore, combining detailed core analysis with petrophysical data over the erg-lacustrine transition is crucial for improving understanding of reservoir characterization, particularly when these targeting depositional environments are found below extensive salt deposits, like the Zechstein Supergroup, where seismic resolution is often of poor quality. Understanding reservoir heterogeneities from facies scale to depositional environment scale is vital for predicting fluid migration pathways and potential plume geometries for CO<sub>2</sub> storage (Sundal *et al.* 2013). The intraformational seals can cause capillary trapping of CO<sub>2</sub>, thus increasing the potential CO<sub>2</sub> storage capacity (Krevor *et al.* 2015), however they can also complicate CO<sub>2</sub> plume predictions, and impact the overall storage volumes.

Facies maps (Fig. 8) suggest that the east of the studied area would be optimal for CCS storage within the formation. Natural CO<sub>2</sub> reservoirs have already been identified within the Lower Permian Rotliegend Group, namely the Fizzy and Oak fields in

blocks 49/30, 50/26 and 54/1 (Heinemann *et al.* 2013; Miocic *et al.* 2014), with the extensive lacustrine mudstones deposited during repetitive transgressions of the saline lake forming the initial intraformational seals for CO<sub>2</sub> storage, and the Zechstein salt Supergroup forming the more regional overarching secondary seal. Well 49/11a-4 for example, shows multiple periods of transgression and regression of the desert lake system over aeolian dunefields (Fig. 9). This results in a series of potential storage reservoirs of high permeability and porosity sandstones intercalated with intervals with good sealing potential due to the present of impermeable sediment and heterogeneous strata. This is counterintuitive to traditional hydrocarbon exploration zones present towards the south of the studied area (well 49/26-A6) where multiple stacked, quartz-rich, well-sorted, well-rounded aeolian dune sandstones are observed (Fig. 9). CO<sub>2</sub> storage within these reservoirs would also be a viable option due to potential to store greater volumes of CO<sub>2</sub>, however, the sealing potential of these reservoirs would need to be critically evaluated and areas with potential sealed faults selected to act as initial seals below the overarching Zechstein salt seal.

Secondary targets could also include the centre of the studied area, where there is a well-developed fluvial corridor punctuating the aeolian dune field and interacting with the Silverpit desert lake (well 48/7b-8; Fig. 9). The lateral migration as well as progradation and retrogradation of the fluvial system within this area, along with the expansion and contraction of the desert lake resulted in the complex interplay between the depositional environments adding heterogeneity and potential intraformational seals to an otherwise sandstone rich reservoir. However, the fluvial sediment ranges from heavily recycled aeolian-sourced sediment to mud-rich, matrix and clast-supported conglomerates of both intraformational and extraformational clasts which can cause complications with CO<sub>2</sub> plume migration predictions, as the 'cleaner' aeolian-sourced sandstones could act as preferential pathways for fluid migration.

## Conclusions

The Leman Sandstone, previously explored for hydrocarbons, has the potential to provide new opportunities within carbon capture and storage to help meet 'net zero' targets by 2050. The wealth of open access data, particularly core, available from the North Sea allows for detailed reassessment of depleted reservoirs. The Leman Sandstone comprises sediments deposited within aeolian, fluvial and lacustrine environments. Complex interactions are observed between these environments as a result of cyclic transgressions and regressions of the aeolian and lacustrine settings, along with the migration and expansion of the fluvial system. Each depositional environment, along with their transitional, interacting environments, have relatively distinct petrophysical properties and cross-plot clusters which can be used to extrapolate data for wells without core. This ability to constrain the mixed aeolian-lacustrine depositional belt is important, as it represents an ideal storage site for CCS, though has previously been overlooked for conventional exploration due to complex interactions between depositional environments resulting in multiple intraformational seals within the reservoir units. Our findings ultimately highlight a bias in wellbore datasets towards higher net to gross depositional settings, than lower net, mixed systems potentially more favourable to CCS due to capillary trapping of CO<sub>2</sub>.

**Acknowledgements** The sedimentological analysis for the study was undertaken during a PhD research project as part of the Natural Environment Research Council (NERC) Centre for Doctoral Training (CDT) in Oil & Gas under its Extending the Life of Mature Basins theme [grant number: NEM00578X/1]. It was sponsored by NERC and the British Geological Survey (BGS) via the British University Funding Initiative (BUFI) whose support is gratefully acknowledged. We are also thankful to the BGS at Keyworth for access to the core store, and the UK National Data Repository (NDR) for access to

the well data. We are grateful to Schlumberger for licensed use of Petrel software at the University of Aberdeen. We would also like to thank the reviewers: Conxita Taberner, Gokturk Mehmet Dilci, Mark Bentley, and one anonymous reviewer for their constructive feedback that has helped improve the manuscript.

**Author contributions** CLP: conceptualization (lead), data curation (equal), formal analysis (lead), writing – original draft (lead); RPP: conceptualization (supporting), data curation (supporting), formal analysis (supporting), writing – original draft (supporting), writing – review & editing (equal); DW: data curation (supporting), software (equal), writing – review & editing (equal); AVR: data curation (equal), writing – review & editing (equal); SMC: funding acquisition (lead), supervision (lead), writing – review & editing (equal)

**Funding** This work was funded by the Natural Environment Research Council (NEM00578X/1) and British Geological Survey.

**Competing interests** The authors declare that they have no known competing financial interests or personal relationships that could have appeared to influence the work reported in this paper.

**Data availability** The data that support the findings of this study are available from the corresponding author upon reasonable request.

## References

- Abdullatif, O.M. 1989. Channel-fill and sheet-flood facies sequences in the ephemeral terminal River Gash, Kassala, Sudan. *Sedimentary Geology*, **63**, 171–184, [https://doi.org/10.1016/0037-0738\(89\)90077-8](https://doi.org/10.1016/0037-0738(89)90077-8)
- Allen, J.R.L. 1963. The classification of cross-stratified units, with notes on their origin. *Sedimentology*, **2**, 93–114, <https://doi.org/10.1111/j.1365-3091.1963.tb01204.x>
- Andrews, S.D. and Hartley, A.J. 2015. The response of lake margin sedimentary systems to climatically driven lake level fluctuations: Middle Devonian, Orcadian Basin, Scotland. *Sedimentology*, **62**, 1693–1716, <https://doi.org/10.1111/sed.12200>
- Arnott, R.W.C. and Hand, B.M. 1989. Bedforms, primary structures and grain fabric in the presence of suspended sediment rain. *Journal of Sedimentary Research*, **59**, 1062–1069, <https://doi.org/10.1306/212F90F2-2B24-11D7-8648000102C1865D>
- Arthur, T.J., Pilling, D., Bush, D. and Macchi, L. 1986. The Leman Sandstone Formation in UK Block 49/28 sedimentation, diagenesis and burial history. *Geological Society, London, Special Publications*, **23**, 251–266, <https://doi.org/10.1144/GSL.SP.1986.023.01.16>
- Bailey, R.J. and Lloyd, D.A. 2001. A log correlation of the Rotliegend of the northern Cleaver Bank High: the search for controls on reservoir sand distribution. *Petroleum Geoscience*, **7**, 351–358, <https://doi.org/10.1144/petgeo.7.4.351>
- Bentham, M., Williams, G., Vosper, H., Chadwick, A., Williams, J. and Kirk, K. 2017. Using pressure recovery at a depleted gas field to understand saline aquifer connectivity. *Energy Procedia*, **114**, 2906–2920, <https://doi.org/10.1016/j.egypro.2017.03.1418>
- Besly, B., Romain, H.G. and Mountney, N.P. 2018. Reconstruction of linear dunes from ancient aeolian successions using subsurface data: Permian Auk Formation, Central North Sea, UK. *Marine and Petroleum Geology*, **91**, 1–18, <https://doi.org/10.1016/j.marpetgeo.2017.12.021>
- Billi, P. 2007. Morphology and sediment dynamics of ephemeral stream terminal distributary systems in the Kobo Basin (northern Welo, Ethiopia). *Geomorphology*, **85**, 98–113, <https://doi.org/10.1016/j.geomorph.2006.03.012>
- Boggs, S., Jr and Boggs, S. 2009. *Petrology of Sedimentary Rocks*. 2nd edn. Boggs, S., Jr (ed.) Cambridge University Press, Edinburgh Building, Cambridge.
- Bridge, J.S. 1984. Large-scale facies sequences in alluvial overbank environments. *Journal of Sedimentary Research*, **54**, 85–170, <https://doi.org/10.1306/212F8477-2B24-11D7-8648000102C1865D>
- Bridge, J.S. 2003. *Rivers and Floodplains: Forms, Processes, and Sedimentary Record*. Blackwell Scientific Publishing, 491.
- Bristow, C., Skelly, R. and Ethridge, F. 1999. Crevasse splays from the rapidly aggrading, sand-bed, braided Niobrara River, Nebraska: effect of base-level rise. *Sedimentology*, **46**, 1029–1048, <https://doi.org/10.1046/j.1365-3091.1999.00263.x>
- Butler, J.B. 1975. The west sole gas-field. In: Woodland, A.W. (ed.) *Petroleum and the Continental Shelf of North-West Europe*. Institute of Petroleum Geology, London, 213–223.
- Cameron, T.D.J., Crosby, A., Balson, P.S., Jeffery, D.H., Lott, G.K., Bulat, J. and Harrison, D.J. 1992. *United Kingdom Offshore Regional Report: The Geology of the Southern North Sea*. HMSO for the British Geological Survey, London.
- Carling, P.A. 2013. Freshwater megaflood sedimentation: what can we learn about generic processes? *Earth-Science Reviews*, **125**, 87–113, <https://doi.org/10.1016/j.earscirev.2013.06.002>
- Department for Energy Security & Net Zero 2023. Update to industry on conclusion of the CCUS Cluster Sequencing Track-2 expression of interest, <https://www.gov.uk/government/publications/cluster-sequencing-for-carbon-capture-usage-and-storage-ccus-track-2/update-to-industry-on-conclusion-of-the-ccus-cluster-sequencing-track-2-expression-of-interest> [last accessed 22 August 2023].
- Eaton, T.T. 2006. On the importance of geological heterogeneity for flow simulation. *Sedimentary Geology*, **184**, 187–201, <https://doi.org/10.1016/j.sedgeo.2005.11.002>
- Eberth, D.A. and Miall, A.D. 1991. Stratigraphy, sedimentology and evolution of a vertebrate-bearing, braided to anastomosed fluvial system, Cutler Formation (Permian-Pennsylvanian), north-central New Mexico. *Sedimentary Geology*, **72**, 225–252, [https://doi.org/10.1016/0037-0738\(91\)90013-4](https://doi.org/10.1016/0037-0738(91)90013-4)
- Fielding, C.R. 2006. Upper flow regime sheets, lenses and scour fills: extending the range of architectural elements for fluvial sediment bodies. *Sedimentary Geology*, **190**, 227–240, <https://doi.org/10.1016/j.sedgeo.2006.05.009>
- Fryberger, S.G., Schnek, C.J. and Krystinik, L.F. 1988. Stokes surfaces and the effects of near-surfaces groundwater-table on aeolian deposition. *Sedimentology*, **35**, 21–41, <https://doi.org/10.1111/j.1365-3091.1988.tb00903.x>
- Fyfe, L.J.C. and Underhill, J.R. 2023a. A regional geological overview of the Upper Permian Zechstein Supergroup (Z1 to Z3) in the SW margin of the Southern North Sea and Onshore Eastern England. *Journal of Petroleum Geology*, **46**, 223–256, <https://doi.org/10.1111/jpg.12837>
- Fyfe, L.J. and Underhill, J.R. 2023b. The Upper Permian Zechstein Supergroup of NE England and the adjacent Southern North Sea: a review of its role in the UK's energy transition. *Journal of Petroleum Geology*, **46**, 383–406, <https://doi.org/10.1111/jpg.12843>
- Gast, R.E., Dugar, M. et al. 2010. Rotliegend. In: Doornbal, J.C. and Stevenson, A.G. (eds) *Petroleum Geological Atlas of the Southern Permian Basin Area*. EAGE Publications, Houten, The Netherlands, 101–121.
- George, G.T. and Berry, J.K. 1993. A new lithostratigraphy and depositional model for the Upper Rotliegend of the UK Sector of the Southern North Sea. In: North, C.P. and Prosser, D.J. (eds) *Characterisation of Fluvial and Aeolian Reservoirs*. Geological Society, London, Special Publications, **73**, 291–319, <https://doi.org/10.1144/GSL.SP.1993.073.01.18>
- Glennie, K.W. 1972. Permian Rotliegendes of north-west Europe interpreted in light of modern desert sedimentation studies. *AAPG Bulletin*, **56**, 1048–1071, <https://doi.org/10.1306/819A40AE-16C5-11D7-8645000102C1865D>
- Glennie, K.W. 1983. Early Permian (Rotliegendes) palaeowinds of the North Sea. *Sedimentary Geology*, **34**, 245–265, [https://doi.org/10.1016/0037-0738\(83\)90088-X](https://doi.org/10.1016/0037-0738(83)90088-X)
- Glennie, K.W. 1986. Development of NW Europe's Southern Permian gas basin. In: Brooks, J., Goff, J. and van Hooorn, B. (eds) *Habitat of Palaeozoic Gas in Northwest Europe*. Geological Society, London, Special Publications, **23**, 3–22, <https://doi.org/10.1144/GSL.SP.1986.023.01.01>
- Glennie, K.W. 1998. Lower Permian-Rotliegend. In: Glennie, K.W. (ed.) *Petroleum Geology of the North Sea: Basic Concepts and Recent Advances*. Blackwell Science, Oxford, 137–173, <https://doi.org/10.1002/9781444313413.ch5>
- Glennie, K.W., Mudd, G.C. and Nagtegaal, P.J.C. 1978. Depositional environment and diagenesis of Permian Rotliegendes sandstones in Leman Bank and Sole Pit areas of the UK southern North Sea. *Journal of the Geological Society*, **135**, 25–34, <https://doi.org/10.1144/gsjgs.135.1.0025>
- Gluysas, J.G. and Bagudu, U. 2020. The endurance CO<sub>2</sub> storage site, blocks 42/25 and 43/21, UK North Sea. *Geological Society, London, Memoirs*, **52**, 163–171, <https://doi.org/10.1144/M52-2019-47>
- Grant, R.J., Underhill, J.R., Hernández-Casado, J., Barker, S.M. and Jamieson, R.J. 2019. Upper Permian Zechstein Supergroup carbonate-evaporite platform palaeomorphology in the UK southern North Sea. *Marine and Petroleum Geology*, **100**, 484–518, <https://doi.org/10.1016/j.marpetgeo.2017.11.029>
- Guan, Q., Wang, L., Wang, F., Pan, B., Song, N., Li, F. and Lu, M. 2016. Phosphorus in the catchment of high sediment load river: a case of the Yellow River, China. *Science of The Total Environment*, **572**, 660–670, <https://doi.org/10.1016/j.scitotenv.2016.06.125>
- Heinemann, N., Wilkinson, M., Haszeldine, R.S., Fallick, A.E. and Pickup, G.E. 2013. CO<sub>2</sub> sequestration in a UK North Sea analogue for geological carbon storage. *Geology*, **41**, 411–414, <https://doi.org/10.1130/G33835.1>
- Hillier, A.P. and Williams, B.P.J. 1991. The Leman field, blocks 49/26, 49/27, 49/28, 53/1, 53/2, UK North Sea. *Geological Society, London, Memoirs*, **14**, 451–458, <https://doi.org/10.1144/GSL.MEM.1991.014.01.56>
- HM Government 2021. UK Hydrogen Strategy, [https://assets.publishing.service.gov.uk/government/uploads/system/uploads/attachment\\_data/file/1175494/UK-Hydrogen-Strategy\\_web.pdf](https://assets.publishing.service.gov.uk/government/uploads/system/uploads/attachment_data/file/1175494/UK-Hydrogen-Strategy_web.pdf) [last accessed 18 August 2023].
- Hollingsworth, A.D., de Jonge-Anderson, I., Underhill, J.R. and Jamieson, R.J. 2022. Geological evaluation of suprasalt carbon storage opportunities in the Silverpit Basin, United Kingdom Southern North Sea. *AAPG Bulletin*, **106**, 1791–1825, <https://doi.org/10.1306/03232221119> [COMP: note updates to Hollingsworth et al. 2022]
- Howell, J. and Mountney, N. 1997. Climatic cyclicity and accommodation space in arid to semi-arid depositional systems: an example from the Rotliegend Group of the UK southern North Sea. In: Fleet, A.J. (ed.) *Petroleum Geology*

- of the Southern North Sea: Future Potential. Geological Society, London, Special Publications, **123**, 63–86, <https://doi.org/10.1144/GSL.SP.1997.123.01.05>
- Hunter, R.E. 1977a. Basic types of stratification in small eolian dunes. *Sedimentology*, **24**, 361–387, <https://doi.org/10.1111/j.1365-3091.1977.tb00128.x>
- Hunter, R.E. 1977b. Terminology of cross-stratified sedimentary layers and climbing ripple structures. *Journal of Sedimentary Petrology*, **47**, 697–706, <https://doi.org/10.1306/212F7225-2B24-11D7-8648000102C1865D>
- Jagger, A. 2003. *Sedimentology and Stratigraphic Evolution of the Permian Cedar Mesa Sandstone, SE Utah*. Unpublished PhD thesis, University of Keele, Keele, 391.
- Jolley, S.J., Fisher, Q.J. and Ainsworth, R.B. 2010. Reservoir compartmentalization: an introduction. *Geological Society, London, Special Publications*, **347**, 1–8, <https://doi.org/10.1144/SP347.1>
- Kocurek, G. 1991. Interpretation of ancient eolian sand dunes. *Annual Review of Earth and Planetary Sciences*, **19**, 43–75, <https://doi.org/10.1146/annurev.earth.19.050191.000355>
- Kocurek, G. 1996. Desert aeolian systems. In: Reading, H.G. (ed.) *Sedimentary Environments: Processes, Facies and Stratigraphy*. 3rd edn. Blackwell Science Ltd, Cambridge, 125–153.
- Kocurek, G. and Nielson, J. 1986. Conditions favorable for the formation of warm-climate aeolian sand sheets. *Sedimentology*, **33**, 795–816, <https://doi.org/10.1111/j.1365-3091.1986.tb00983.x>
- Krevor, S., Blunt, M.J., Benson, S.M., Pentland, C.H., Reynolds, C., Al-Menhali, A. and Niu, B. 2015. Capillary trapping for geologic carbon dioxide storage—From pore scale physics to field scale implications. *International Journal of Greenhouse Gas Control*, **40**, 221–237, <https://doi.org/10.1016/j.ijggc.2015.04.006>
- Lang, J. and Winsemann, J. 2013. Lateral and vertical facies relationships of bedforms deposited by aggrading supercritical flows: from cyclic steps to humpback dunes. *Sedimentary Geology*, **296**, 36–54, <https://doi.org/10.1016/j.sedgeo.2013.08.005>
- Langford, R.P. and Chan, M.A. 1989. Fluvial-aeolian interactions: part II, ancient systems. *Sedimentology*, **36**, 1037–1051, <https://doi.org/10.1111/j.1365-3091.1989.tb01541.x>
- Marie, J.P.P. 1975. Rotliegendes stratigraphy and diagenesis. In: Woodland, A.W. (ed.) *Petroleum and the Continental Shelf of North-West Europe*. Applied Science Publishers, Barking, 205–210.
- McKay, C.P., Rask, J.C., Detweiler, A.M., Bebout, B.M., Everroad, R.C., Lee, J.Z. and Al-Awar, M. 2016. An unusual inverted saline microbial mat community in an interdune sabkha in the Rub' al Khali (the Empty Quarter), United Arab Emirates. *PLoS One*, **11**, e0150342, <https://doi.org/10.1371/journal.pone.0150342>
- Metcalfe, R., Thatcher, K., Towler, G., Paulley, A. and Eng, J. 2017. Sub-surface risk assessment for the Endurance CO<sub>2</sub> Store of the White Rose Project, UK. *Energy Procedia*, **114**, 4313–4320, <https://doi.org/10.1016/j.egypro.2017.03.1578>
- Miall, A.D. 1988. Architectural elements and bounding surfaces in fluvial deposits: anatomy of the Kayenta Formation (Lower Jurassic), southwest Colorado. *Sedimentary Geology*, **55**, 233–262, [https://doi.org/10.1016/0037-0738\(88\)90133-9](https://doi.org/10.1016/0037-0738(88)90133-9)
- Miocic, J.M., Johnson, G. and Gilfillan, S.M. 2014. Fault seal analysis of a natural CO<sub>2</sub> reservoir in the Southern North Sea. *Energy Procedia*, **63**, 3364–3370, <https://doi.org/10.1016/j.egypro.2014.11.365>
- Moscariello, A. 2011. Sedimentary facies, correlation, and architecture of Rotliegend reservoirs at the Southern Permian basin margin: the P01-FA case study and the challenged myth of layer-cake stratigraphy. *SEPM Special Publication*, **98**, 177–190, <https://doi.org/10.2110/pec.11.98.0177>
- Mountney, N.P. and Jagger, A. 2004. Stratigraphic evolution of an aeolian erg margin system: the Permian Cedar Mesa Sandstone, SE Utah, USA. *Sedimentology*, **51**, 713–743, <https://doi.org/10.1111/j.1365-3091.2004.00646.x>
- Mullins, J., Pierce, C., Rieke, H. and Howell, J. 2022. Aeolian sand dune sedimentary architecture is key in determining the 'slow gas effect' during gas field production performance. *SPE Journal*, **27**, 1354–1366, <https://doi.org/10.2118/208617-PA>
- Nielsen, P. 1981. Dynamics and geometry of wave-generated ripples. *Journal of Geophysical Research*, **86**, 6467–6472, <https://doi.org/10.1029/JC086iC07p06467>
- NSTA 2022. Net zero boost as carbon storage licenses accepted, <https://www.nstauthority.co.uk/news-publications/net-zero-boost-as-carbon-storage-licences-accepted/> [last accessed 26 October 2022].
- NSTA 2023. Overview 2023, <https://www.nstauthority.co.uk/media/imofibq1/a5la5overview-oeupdate23-final-accessible.pdf?fbclid=IwAR1G1jdGtVe-q37fLLU4PeeCV-4abHYrti4T8wCDUKnR9g7ag8H9-4Stws> [last accessed 24 November 2023]
- OGUK 2021. North Sea Transition Deal, [https://assets.publishing.service.gov.uk/government/uploads/system/uploads/attachment\\_data/file/972520/north-sea-transition-deal\\_FINAL.pdf](https://assets.publishing.service.gov.uk/government/uploads/system/uploads/attachment_data/file/972520/north-sea-transition-deal_FINAL.pdf) [last accessed 18 August 2023].
- OGUK 2022. North Sea Transitional Deal One Year On, [https://assets.publishing.service.gov.uk/government/uploads/system/uploads/attachment\\_data/file/1061986/north-sea-transition-deal-one-year-on.pdf](https://assets.publishing.service.gov.uk/government/uploads/system/uploads/attachment_data/file/1061986/north-sea-transition-deal-one-year-on.pdf) [last accessed 18 August 2023].
- Oil & Gas Authority 2021. OGA grants carbon storage licence to Harbour Energy, <https://www.nstauthority.co.uk/news-publications/news/2021/oga-grants-carbon-storage-licence-to-harbour-energy/> [last accessed 19 July 2022].
- Pettigrew, R.P., Rogers, S.L. and Clarke, S.M. 2020. A microfacies analysis of arid continental carbonates from the Cedar Mesa Sandstone Formation, Utah, USA. *The Depositional Record*, **6**, 41–61, <https://doi.org/10.1002/dep2.99>
- Pettigrew, R.P., Priddy, C., Clarke, S.M., Warke, M.R., Stüeken, E.E. and Claire, M.W. 2021. Sedimentology and isotope geochemistry of transitional evaporitic environments within arid continental settings: from erg to saline lakes. *Sedimentology*, **68**, 907–942, <https://doi.org/10.1111/sed.12816>
- Priddy, C.L. 2021. *The Sedimentary Architecture and Spatial Variations of Dryland Ephemeral Fluvial Systems*. PhD thesis, Keele University.
- Priddy, C.L. and Clarke, S.M. 2020. The sedimentology of an ephemeral fluvial-aeolian succession. *Sedimentology*, **67**, 2392–2425, <https://doi.org/10.1111/sed.12706>
- Prosser, D.J. 1988. *The Sedimentology and Diagenesis of Lower Permian (Rotliegend) Sediments: (Onshore UK and Southern North Sea)*. Unpublished PhD thesis, The University of Aston, Birmingham, 1, 39–279.
- Reitner, J. 2011. Microbial mats. In: Reitner, J. and Thiel, V. (eds) *Encyclopedia Geobiology. Part of the Series of Encyclopedia of Earth Sciences*. Springer, Heidelberg, 606–608.
- Sadler, S.P. and Kelly, S.B. 1993. Fluvial processes and cyclicity in terminal fan deposits: an example from the Late Devonian of southwest Ireland. *Sedimentary Geology*, **85**, 375–386, [https://doi.org/10.1016/0037-0738\(93\)90093-K](https://doi.org/10.1016/0037-0738(93)90093-K) [COMP: update Sadler and Kelly 1993 to journal reference]
- Sáez, A., Anadón, P., Herrero, M.J. and Moscardiello, A. 2007. Variable style of transition between Palaeogene fluvial fan and lacustrine systems, southern Pyrenean foreland, NE Spain. *Sedimentology*, **54**, 367–390, <https://doi.org/10.1111/j.1365-3091.2006.00840.x>
- Smoot, J.P. and Lowenstein, T.K. 1991. Depositional environments of non-marine evaporites. In: Melvin, J.L.J. (Ed.) *Developments in Sedimentology*. Elsevier, **50**, 189–347, [https://doi.org/10.1016/S0070-4571\(08\)70261-9](https://doi.org/10.1016/S0070-4571(08)70261-9)
- Sundal, A., Nystuen, J.P., Dypvik, H., Miri, R. and Aagaard, P. 2013. Effects of geological heterogeneity on CO<sub>2</sub> distribution and migration—A case study from the Johansen Formation, Norway. *Energy Procedia*, **37**, 5046–5054, <https://doi.org/10.1016/j.egypro.2013.06.418>
- Sutherland, F., Lawrance, D., Legrand, P. and Wraith, E. 2022. Seismic monitoring for subsurface uncertainties at the Endurance CO<sub>2</sub> store. *The Leading Edge*, **41**, 253–258, <https://doi.org/10.1190/lel41040253.1>
- Sweet 1999. Interaction between aeolian, fluvial and playa environments in the Permian Upper Rotliegend Group, UK southern North Sea. *Sedimentology*, **46**, 171–187, <https://doi.org/10.1046/j.1365-3091.1999.00211.x>
- Tooth, S. 1999. Downstream changes in floodplain character on the Northern Plains of arid central Australia. In: Smith, N.D. and Rogers, J. (eds) *Fluvial Sedimentology VI. International Association of Sedimentologists, Special Publication*, **28**. Blackwell, Oxford, 93–112, <https://doi.org/10.1002/9781444304213.ch8>
- Tooth, S. 2000. Process, form and change in dryland rivers: a review of recent research. *Earth-Science Reviews*, **51**, 67–107, [https://doi.org/10.1016/S0012-8252\(00\)00014-3](https://doi.org/10.1016/S0012-8252(00)00014-3)
- Tooth, S. 2005. Splay formation along the lower reaches of ephemeral rivers on the Northern Plains of arid central Australia. *Journal of Sedimentary Research*, **75**, 636–649, <https://doi.org/10.2110/jsr.2005.052>
- Underhill, J.R. 2003. The tectonic and stratigraphic framework of the United Kingdom's oil and gas fields. *Geological Society, London, Memoirs*, **20**, 17–59, <https://doi.org/10.1144/GSL.MEM.2003.020.01.04>
- Underhill, J.R., de Jonge-Anderson, I., Hollinsworth, A.D. and Fyfe, L.C. 2023. Use of exploration methods to repurpose and extend the life of a super basin as a carbon storage hub for the energy transition. *AAPG Bulletin*, **107**, 1419–1474, <https://doi.org/10.1306/04042322097>
- United Nations 2015. Paris Agreement, [https://unfccc.int/sites/default/files/english\\_paris\\_agreement.pdf](https://unfccc.int/sites/default/files/english_paris_agreement.pdf) [last accessed 18 August 2023].
- Van Dover, C.L. 2000. *The Ecology of Deep-Sea Hydrothermal Vents*. Princeton University Press, Princeton, 424.
- Van Hoorn, B. 1987. Structural evolution, timing and tectonic style of the Sole Pit inversion. *Tectonophysics*, **137**, 239–284, [https://doi.org/10.1016/0040-1951\(87\)90322-2](https://doi.org/10.1016/0040-1951(87)90322-2)
- Van Veen, F.R. 1975. Geology of leman gas-field. *Geology*, **1**, 223–231.
- Warren, J.K. 2006. *Evaporites: Sediments, Resources and Hydrocarbons*. Springer Science & Business Media.
- Weber, K.J. 1988. Computation of initial well productivities in aeolian sandstone on the basis of a geological model, Leman gas field, UK. In: Tillman, R.W. and Weber, K.J. (eds) *Reservoir Sedimentology. SEPM Special Publication*, **40**, 333–354, <https://doi.org/10.2110/pec.87.40.0333>